European Journal of Medicinal Chemistry 261 (2023) 115803

Contents lists available at ScienceDirect

European Journal of Medicinal Chemistry

journal homepage: www.elsevier.com/locate/ejmech

Research paper

Galantamine-memantine hybrids for Alzheimer's disease: The influence of linker rigidity in biological activity and pharmacokinetic properties

Filippo Basagni [a], Jose A. Ortega [b], Sine M. Bertozzi [c], Andrea Armirotti [c], Maria Summa [d], Rosalia Bertorelli [d], Manuela Bartolini [a], Ian R. Mellor [e], Martina Bedeschi [a,e], Giovanni Bottegoni [f,g], Vittorio Lembo [b,f], Anna Minarini [a], Andrea Cavalli [a,b,**], Michela Rosini [a,*]

[a] Department of Pharmacy and Biotechnology, Alma Mater Studiorum – University of Bologna, Via Belmeloro 6, 40126, Bologna, Italy
[b] Computational and Chemical Biology, Istituto Italiano di Tecnologia, Via Morego 30, 16163, Genova, Italy
[c] Analytical Chemistry Facility, Istituto Italiano di Tecnologia, Via Morego 30, 16163, Genova, Italy
[d] Translational Pharmacology Facility, Istituto Italiano di Tecnologia, Via Morego 30, 16163, Genova, Italy
[e] School of Life Sciences, University of Nottingham, University Park, Nottingham, NG7 2RD, UK
[f] Department of Biomolecular Sciences, University of Urbino "Carlo Bo", Piazza Rinascimento 6, 61029, Urbino, Italy
[g] Institute of Clinical Sciences, University of Birmingham, Edgbaston, B15 2TT, Birmingham, UK

ARTICLE INFO

Keywords:
Alzheimer's disease
Galantamine
Memantine
Drug conjugate
Cholinesterases
NMDAR

ABSTRACT

Neurodegenerative processes characterizing Alzheimer's disease (AD) are strictly related to the impairment of cholinergic and glutamatergic neurotransmitter systems which provoke synaptic loss. These experimental evidences still represent the foundation of the actual standard-of-care treatment for AD, albeit palliative, consisting on the coadministration of an acetylcholinesterase inhibitor and the NMDAR antagonist memantine. In looking for more effective treatments, we previously developed a series of galantamine-memantine hybrids where compound **1** (ARN14140) emerged with the best-balanced action toward the targets of interest paired to neuroprotective efficacy in a murine AD model. Unfortunately, it showed a suboptimal pharmacokinetic profile, which required intracerebroventricular administration for *in vivo* studies. In this work we designed and synthesized new hybrids with fewer rotatable bonds, which is related to higher brain exposure. Particularly, compound **2**, bearing a double bond in the tether, ameliorated the biological profile of compound **1** in *in vitro* studies, increasing cholinesterases inhibitory potencies and selective antagonism toward excitotoxic-related GluN1/2B NMDAR over beneficial GluN1/2A NMDAR. Furthermore, it showed increased plasma stability and comparable microsomal stability *in vitro*, paired with lower half-life and faster clearance *in vivo*. Remarkably, pharmacokinetic evaluations of compound **2** showed a promising increase in brain uptake in comparison to compound **1**, representing the starting point for further chemical optimizations.

1. Introduction

Alzheimer's disease (AD) is a chronic neurodegenerative condition characterized by loss of neuronal cells and impaired neurotransmission. Evidence exists for both cholinergic and glutamatergic involvement in AD, leading to the two major classes of agents currently on the market to treat cognitive symptoms in AD patients. The acetylcholinesterase (AChE) inhibitors (AChEIs) donepezil, rivastigmine and galantamine improve cholinergic neurotransmission by increasing acetylcholine (ACh) levels in the brain, while the noncompetitive *N*-methyl-D-aspartate (NMDA) receptor (NMDAR) antagonist memantine restores glutamatergic signaling by reducing excessive NMDAR activity that leads to excitotoxicity. Multifaceted functional interactions occur between cholinergic and glutamatergic pathways [1], suggesting that treatment strategies should concurrently address impairments in both systems. Thus, the co-administration of an AChE inhibitor with memantine (as cocktails or multicomponent drugs) currently represents the standard of care in AD [2]. As a natural evolution of this concept, the development of a single molecule that can simultaneously hit both targets has recently

* Corresponding author. Department of Pharmacy and Biotechnology, Alma Mater Studiorum – University of Bologna, Via Belmeloro 6, 40126, Bologna, Italy.
** Corresponding author. Department of Pharmacy and Biotechnology, Alma Mater Studiorum – University of Bologna, Via Belmeloro 6, 40126, Bologna, Italy.
E-mail addresses: andrea.cavalli@unibo.it (A. Cavalli), michela.rosini@unibo.it (M. Rosini).

https://doi.org/10.1016/j.ejmech.2023.115803
Received 11 July 2023; Received in revised form 6 September 2023; Accepted 7 September 2023
Available online 12 September 2023

Abbreviations

ACh	acetylcholine
AChE	acetylcholinesterase
AChEI	acetylcholinesterase inhibitor
AD	Alzheimer's disease
ADME	absorption, distribution, metabolism and excretion
BBB	blood-brain barrier
BChE	butyrylcholinesterase
ChE	cholinesterase
CNS	central nervous system
DIBAL-H:	diisobutylaluminum hydride
eNMDAR	extrasynaptic NMDAR
G6P	glucose-6-phosphate
G6PDH	glucose-6-phosphate dehydrogenase
i.c.v.	intracerebroventricular
I.V.	intravenous
MEM	memantine
MRM	multiple reaction monitoring
nAChR	nicotinic acetylcholine receptor
NADPH	nicotinamide adenine dinucleotide phosphate
NMDAR	*N*-methyl-D-aspartate receptor
GluN1	NMDA receptor subunit 1
GluN2A	NMDA receptor subunit 2A
GluN2B	NMDA receptor subunit 2B
Ppm	parts per millions
NMR	nuclear magnetic resonance spectra
PBS	phosphate buffered saline
PDA	photodiode array detector
PK	pharmacokinetic
SI	selectivity index
sNMDAR	synaptic NMDAR
SQD	single quadrupole detector
TBAF	tetrabutylammonium fluoride
TMS	tetramethylsilane
TQD	triple quadrupole detector
UDPGA	uridine 5′-diphospho-glucuronic acid

emerged as a feasible and attractive polypharmacology option [3]. Of particular interest in this respect, we considered the peculiar profile of galantamine, whose ability to sustain cholinergic neurotransmission is accompanied by a neuroprotective activity against glutamate toxicity, possibly arising from the stimulation of nicotinic ACh receptors (nAChRs). The finding that the simultaneous administration of inactive concentrations of memantine and galantamine produced a synergistic action and resulted in full neuroprotective efficacy in rat cortical neurons [4] prompted us to covalently link the two drugs into a single chemical entity, following a dual target design strategy [5]. Among the obtained chimeric compounds, ARN14140 (Compound **1**, Fig. 1), carrying a tetramethylene spacer, was the best compromise between achieving high pharmacological potency and maintaining physico-chemical traits compatible with bioavailability. Compound **1** exhibited a fairly balanced profile in *in vitro* studies, with inhibitory activities towards both AChE and NMDA receptors in the micromolar range. When tested in a non-transgenic murine AD model, in which neurodegeneration and cognitive impairment are triggered by an intracerebroventricular (i.c.v.) injection of oligomeric amyloid beta peptide 25–35 ($A\beta_{25\text{-}35}$), **1** showed to revert neurotoxicity in terms of behavioral tasks and biomarkers [6]. Notably, in this study, **1** was administered by i.c.v. injection because of its unfavorable pharmacokinetic (PK) and low brain penetration rate, as encountered in preliminary PK studies.

However, i.c.v. injection is not a feasible administration route when transferring to humans. Thus, we proposed transdermal iontophoresis as a noninvasive mean to efficiently deliver **1** across the skin to the brain [7]. Besides delivery method efforts, in the present study we sought to pursue structural modification as a useful strategy to enhance blood-brain barrier (BBB) penetration. Drugs acting in the central nervous system (CNS) are commonly characterized by strong rigidity, with fused ring systems and limited rotatable bonds [8]. As the flexible polymethylene linker of **1** contributes to rotatable bond count, we herein decided to address the low BBB permeability of **1** by introducing a double and a triple bond in compounds **2** and **3**, respectively (Fig. 1). The new chimeric compounds were initially studied *in vitro* and in silico at human cholinesterases (ChEs) and NMDARs, to verify how structural modifications would impact the activity at single targets, in comparison to **1**. Then, a preliminary pharmacokinetic and metabolic characterization of compounds **1**–**3** was performed *in vitro* using murine plasma and liver microsomes, followed by brain exposure investigation in CD1 mice.

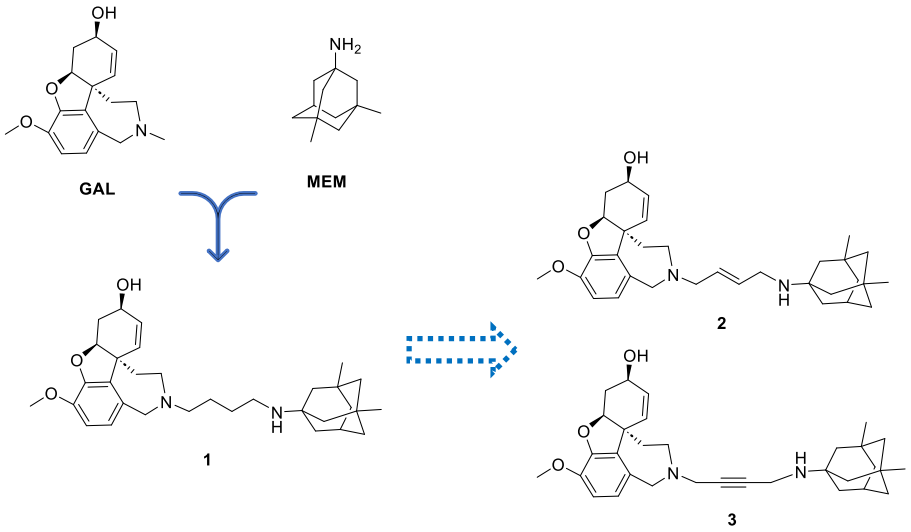

Fig. 1. Drug design strategy for compound **1** and the new stiffened derivatives **2** and **3**.

2. Results and discussion

2.1. Chemistry

Compounds **2** and **3** were obtained following the synthetic routes represented in Schemes 1 and 2. As a common feature, initial chemical functionalization of memantine's adamantane nucleus was employed to insert the proper unsaturated linker, followed by a late-stage conjugation with *N*-desmethyl galantamine. In detail, concerning the synthesis of compound **2** (Scheme 1), memantine free base underwent a microwave-assisted nucleophilic substitution with methyl 4-bromocrotonate achieving intermediate **4**, whose secondary amine function was later Boc-protected (**5**). Reduction of **5**'s ester function with diisobutylaluminum hydride (DIBAL-H) gave alcohol **6**, which was further converted into its chlorinated analogue **7** through an Appel reaction to promote the nucleophilic substitution with *N*-desmethyl galantamine and obtain intermediate **8**. Finally, compound **2** was prepared after carbamate removal under mild acidic condition. The synthetic strategy exploited to obtain compound **3** (Scheme 2) started with the monoprotection of an alcohol moiety of 1,4-butynediol as silyl ether and the activation as tosylate of the other hydroxy function. This produced intermediate **10** that underwent the same two-step microwave-assisted procedure previously reported: a first nucleophilic substitution with memantine followed by a carbamate protection of the secondary amine function. The alcohol moiety of **12** was unmasked after treatment with tetrabutylammonium fluoride (TBAF) and further converted to the easily substitutable tosyl-activated alcohol, necessary for the conjugation of compound **14** with *N*-desmethyl galantamine. Then, HCl-promoted deprotection of the amino group provided compound **3**.

2.2. Cholinesterase inhibition: in vitro and in silico studies

To determine the multitarget profile of compounds **1**–**3**, we initially investigated their inhibitory activity on human recombinant AChE and butyrylcholinesterase (BChE) from human serum by *in vitro* Ellman assay [9]. Galantamine was used as the reference compound (Table 1). Consistent with previously published data on rat AChE [5], compound **1** showed a moderate efficacy (IC_{50} = 1.13 μM) as AChE inhibitor, being two times more potent than galantamine. As for **1**, the hybridization strategy encompassing a four-carbon tether confirmed to be beneficial for AChE inhibition by compounds **2** and **3**. Indeed, both new hybrids showed an improved inhibitory potency towards human AChE when compared to parent compound **1**, with **2** registering a 10-fold boost in potency (IC_{50} = 0.115 *vs* 1.13 μM).

Docking simulations were carried out to analyze the impact of the decreased conformational flexibility of the linker on the binding mode of the new compounds. These simulations were performed on a model structure of AChE obtained by superimposing the donepezil-bound co-crystal to the structure of the human enzyme solved in complex with galantamine (PDB code 4EY6), to use galantamine as a reference in the binding pose prediction of compounds **1**–**3** while retaining the donepezil-bound orientation of the side chains in the binding pocket [11]. These are already adapted to accommodate ligands concurrently contacting both the catalytic site and the peripheral anionic site. According to our results, compounds **1**, **2** (Fig. 2) and **3** (Figure S1) bind at the AChE gorge with an orientation that is consistent with the one adopted by donepezil [11]. The galantamine substructure of our compounds established a hydrophobic interaction with the indole ring of Trp86 and formed H-bond interactions with the side chains of Glu202 and Ser203. The proposed binding mode could explain the increased

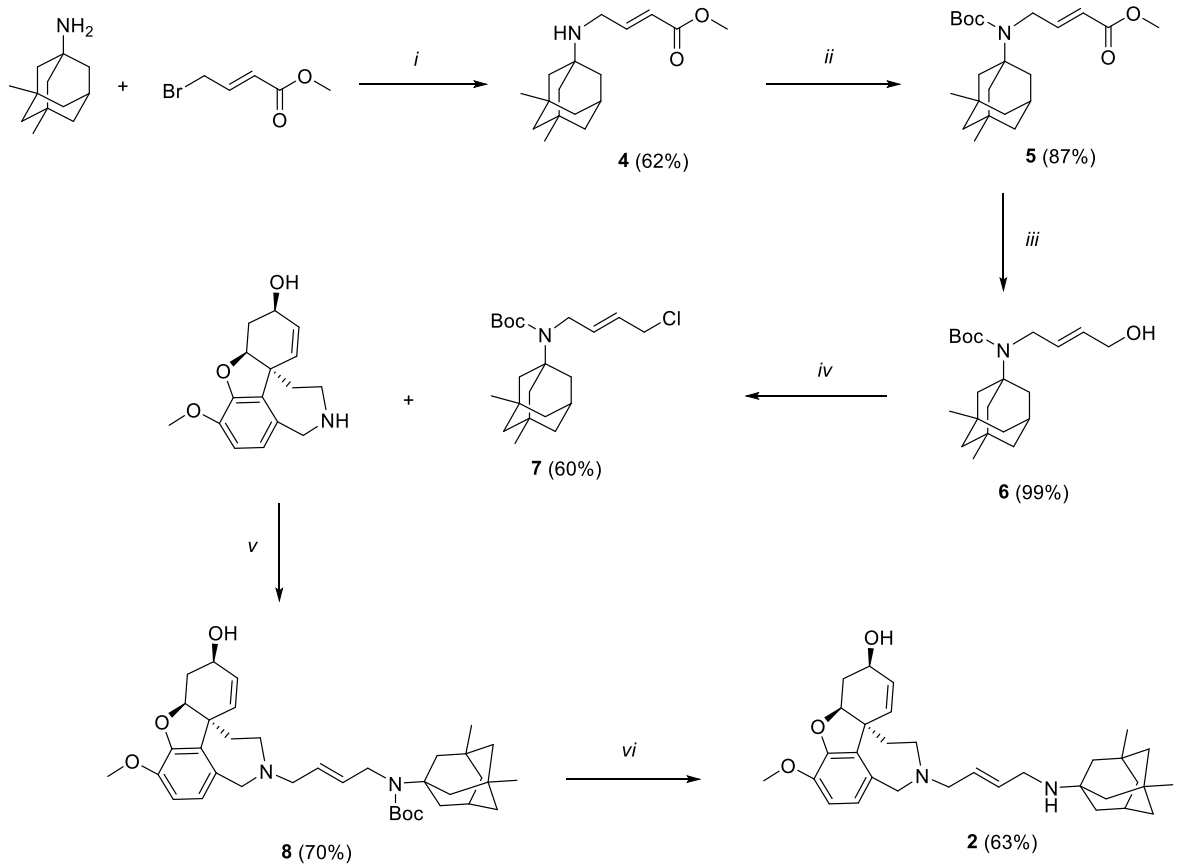

Scheme 1. Synthesis of compound 2[a] Reagents and conditions: *(i)* K_2CO_3, DMF, MW, 60 °C, 10 min; *(ii)* Boc_2O, H_2O/THF, MW, 60 °C, 2 h; *(iii)* DIBAL-H, THF, −78 °C, 4 h; *(iv)* NCS, PPh_3, DCM, 0 °C, 15 min; *(v)* Et_3N, ACN, reflux, 7 h; *(vi)* HCl 4 M in dioxane, 0 °C, 50 min.

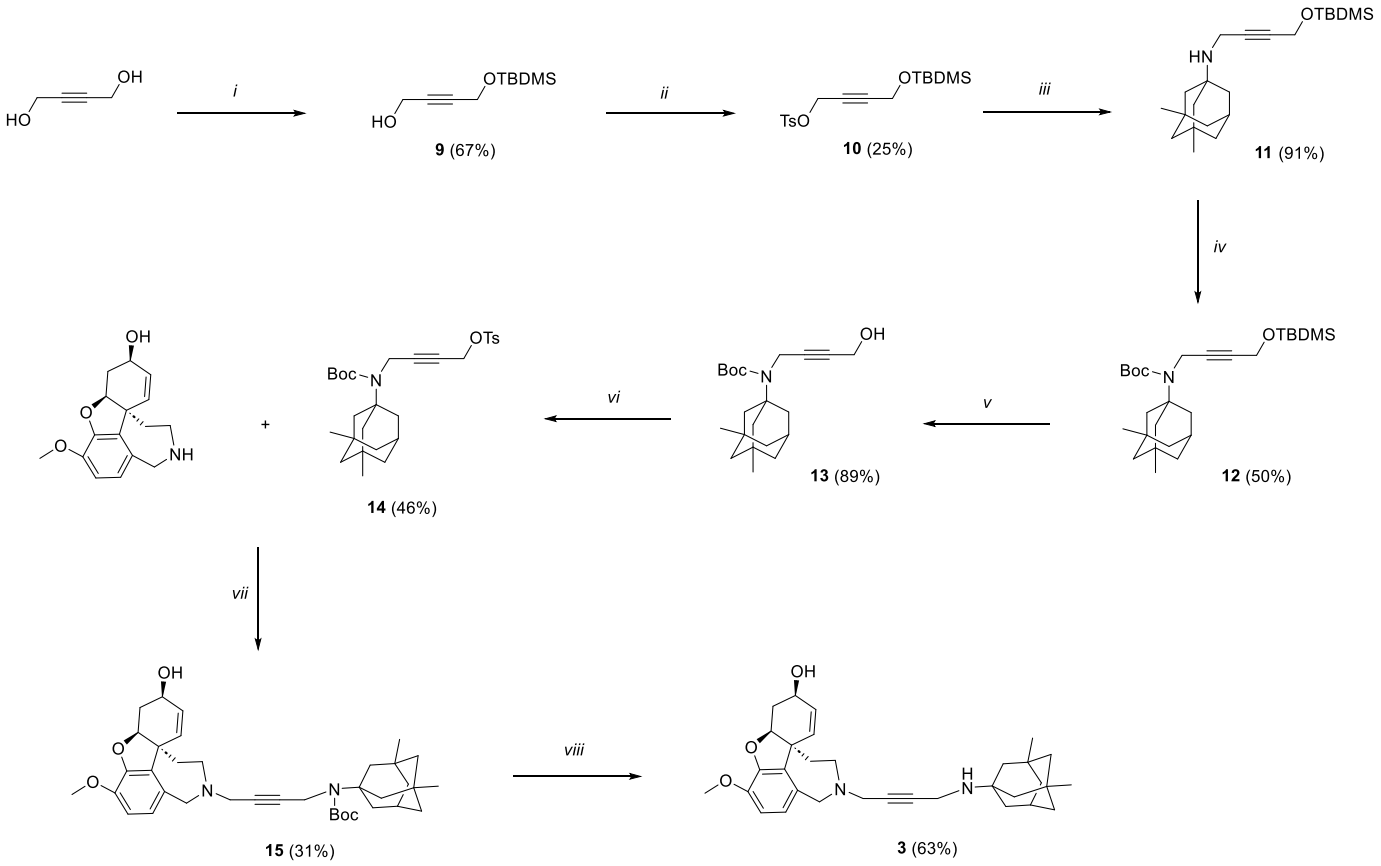

Scheme 2. Synthesis of compound 3[b] Reagents and conditions: *(i)* TBDMSCl, Et_3N, DMF/DCM, 0°C-r.t., 18 h; *(ii)* TsCl, Et_3N, DMAP, DCM, 0°C-r.t., 10 min; *(iii)* memantine, K_2CO_3, DMF, MW, 80 °C, 20 min; *(iv)* Boc_2O, Na_2CO_3, THF/H_2O, MW, 60 °C, 2 h; *(v)* TBAF, THF, N_2, r. t., 30 min; *(vi)* TsCl, Et_3N, DMAP, DCM, 0°C-r.t., 15 min; *(vii)* Et_3N, ACN, reflux, 30 min; *(viii)* HCl 4 M in dioxane, 0 °C, 40 min.

Table 1
ChE and NMDAR inhibition by compounds 1-3.

Cpd	IC_{50} *h*AChE[a] (μM)	IC_{50} *h*BChE[a] (μM)	Selectivity index[b]	IC_{50} NMDAR GluN1/2A[c] [95% CI] (μM)	IC_{50} NMDAR GluN1/2B[c] [95% CI] (μM)	Selectivity index[d]
1	1.13 ± 0.11	1.77 ± 0.19	1.57	5.74 [2.19–14.8]	1.45 [0.81–2.48]	4.0
2	0.115 ± 0.003	0.421 ± 0.036	3.67	14.5 [5.38–44.6]	1.32 [0.24–4.30]	11.0
3	0.762 ± 0.046	5.08 ± 0.07	6.67	11.6 [3.10–70.1]	15.5 [5.38–63.5]	0.75
GAL	2.01 ± 0.15[e]	20.7 ± 1.5[e]	10.30	n.d.	n.d.	–
MEM	n.d.	n.d.	–	2.66 [1.46–4.76]	5.57 [3.54–8.70]	0.48

n.d. stands for not determined.

[a] Data represent mean values ± SEM of at least two experiments each performed in triplicate.

[b] Selectivity index for cholinesterase inhibition. The index was calculated as (BChE IC_{50})/(AChE IC_{50}). Higher SI value corresponds to higher AChE selectivity.

[c] Compounds were tested at NMDAR expressed in *Xenopus laevis* oocytes by the two-electrode voltage clamp technique. Holding potential was −75 mV, NMDARs were activated using NMDA (100 μM) and glycine (10 μM). The IC_{50} obtained was for the steady-state, n = 5–7.

[d] Selectivity index for NMDAR antagonism. The index was calculated as (GluN1/2A IC_{50})/(GluN1/2B IC_{50}). Higher SI value corresponds to higher GluN1/2B selectivity.

[e] Data taken from Ref. [10].

activity of **2** that, thanks to the specific orientation of its linker, can establish two tight interactions of the basic nitrogen of the galantamine moiety and the protonated amine of the adamantane substructure with the side chain of Asp74. The adamantane group also formed a hydrophobic interaction with Trp286. The linker was lodged in a narrow cavity defined by Asp74, Tyr124, Phe297, Tyr337, Phe338, and Tyr341. This orientation can also be adopted by **1**, while its weaker affinity is possibly explained by the increased flexibility of the saturated linker. Finally, while the binding mode of **3** is consistent with that displayed by the other two compounds, the rigidity of the triple bond-bearing linker weakens the interaction between the protonated amine of the adamantane moiety and the side chain of Asp74.

The multimodal cholinergic profile of galantamine includes BChE inhibition in the micromolar range. Like the related enzyme AChE, BChE co-regulates the metabolism of ACh, and its inhibition have been related to strong neuroprotective effects in AD animal models, which highlight it as a potential disease-modifying target [12].

It is generally accepted that as AD progresses, a significant loss of AChE activity in the AD cortex is observed, while increased or stable BChE activity is detected [13]. On this basis, a balanced AChE/BChE action has been proposed to be beneficial, as both enzymes are recognized therapeutic targets at different stages of the pathology [14]. Thus, we also verified the effect of the applied hybridization strategy on BChE inhibition. Interestingly, conjugation with memantine led to a general and significant increase in the inhibitory potency towards BChE with respect to galantamine (Table 1). In particular, compounds **1** and **2**

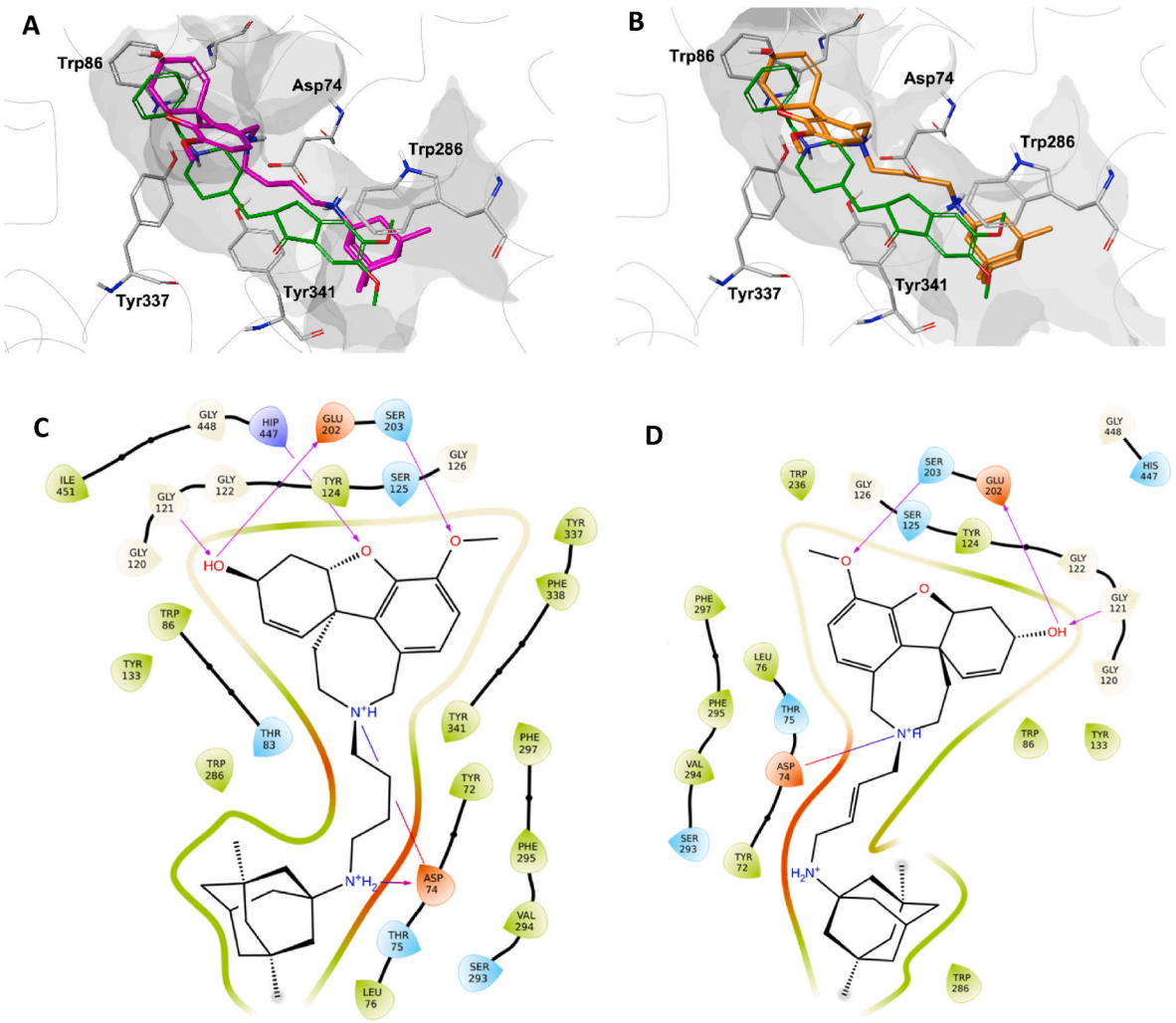

Fig. 2. Predicted binding conformation of compounds **1** (carbon atoms in magenta, A) and **2** (carbon atoms in orange, B) and protein-ligand interactions (*C*-D, respectively) at the binding site of AChE. In panels A–B, the protein structure is reported in thin grey ribbon. Residues interacting with the docked compound are reported in stick representation with light grey carbons and labelled explicitly. The co-crystallised conformation of donepezil is reported for reference (carbon atoms in green). A grey mesh highlights the boundaries of the binding pocket. In panels *C*–D, all residues within 4 Å from the ligand are reported explicitly. Key protein-ligand interactions are depicted as follows: hydrogen bond, purple arrow; salt bridges, red-blue line; π – cation interaction, red circle; solvent exposed atoms are circled in grey.

showed a balanced micromolar or sub-micromolar, respectively, dual AChE/BChE inhibitory activity.

Docking studies into the crystal structure of BChE (PDB code 4BDS) [15] revealed that the orientation adopted by the galantamine sub-structure of the new compounds to the BChE gorge is similar to the one adopted in the AChE binding site (Figures S2-4), while the predicted orientation of the linker and the adamantane moiety of compound **1** and **2** is shifted compared with that predicted in AChE. This can be explained by the larger size of the binding pocket of BChE, where the position corresponding to Trp286 is occupied by Val280, thus allowing for the shifted orientation. A weaker interaction between the basic nitrogen of the adamantane moiety and the side chain of Pro285 could be responsible for the lower affinity of compound **3** (see SI for details). The significant decreased affinity of compound **3** for BChE, when compared to **2**, is also at the basis of the different selectivity profile observed for the most rigid derivative **3**. Indeed, selectivity indexes (SI), defined as the ratio of the inhibitory potency towards BChE over the inhibitory potency towards AChE, for compounds **1** and **2** and **3** were 1.57 and 3.67 and 6.67, respectively. The increased selectivity encountered moving from **2** to **3** is ascribable to a more detrimental effect of the increased structure rigidity on the interaction with BChE than AChE, i.e. selectivity for AChE does not arise from an incremented affinity/activity for/on AChE but from a more pronounced decrement of activity towards BChE. Indeed, while **3** is 6.7 times less potent than **2** towards AChE, when potency towards BChE is considered, **3** results to be 12.1 times less potent than **2**.

2.3. NMDAR antagonism: in vitro and in silico studies

NMDARs are master regulators of neuronal excitatory synaptic transmission that underlies learning and memory, but are also linked to excitotoxicity, which is a pathological state of glutamatergic over-stimulation. The current view is that these conflicting properties are strictly related to receptor localization: activation of synaptic NMDAR (sNMDAR) is beneficial, contributing to cell survival and plasticity, while activation of extrasynaptic NMDAR (eNMDAR) may preferentially signal to neuronal death. Memantine, is a well-tolerated drug specifically directed toward eNMDAR, which are composed predominantly of NMDA receptor 1 (GluN1) and NMDA receptor 2B (GluN2B) subunits, whereas synaptic NMDARs predominantly contain GluN2A subunits [16]. Memantine's specificity of action has been mainly attributed to its open channel blocking properties and favorable kinetics, which allow it to preferentially target extrasynaptic versus synaptic currents, rather

than to its intrinsic NMDAR GluN1/2B selectivity [17]. We and others have previously shown that employing memantine's amine for connecting an auxiliary pharmacophoric appendage can produce only a modest perturbation of memantine's peculiar NMDAR blocking behavior [18]. Herein, guided by the importance of antagonising eNMDARs and preserving the physiological sNMDAR-mediated neurotransmission, we sought to verify if memantine derivatization could offer the chance to selectively recognize GluN1/2B NMDAR over GluN1/2A NMDAR. Thus, we investigated the antagonism of responses to NMDA and glycine elicited by compounds **1**–**3** on GluN2A or GluN2B subunit-containing NMDARs expressed in *Xenopus laevis* oocytes using two-electrode voltage clamp at −75 mV, comparing to memantine as the reference compound (Table 1). Interestingly, conjugation with memantine resulted in a micromolar affinity in the functional assay for all compounds. In particular, compound **1** antagonised at a low micromolar concentration with mild selectivity for GluN2B (SI = ~4). Compound **3** showed a decreased ability to bind to both NMDAR subtypes in comparison to compound **1**, whereas the double bond stiffening of **2** allowed to maintain a low micromolar inhibitory profile toward GluN1/2B with a promising improved selectivity over GluN1/2A receptors (IC_{50} = 1.32 *vs* 14.5 μM, SI = ~11).

In line with previous study [5] and to rationalize GluN2B affinity, compounds **1**–**3** were docked into the crystal structure of the heterodimer formed by the GluN1 and GluN2B subunits of NMDAR, using the coordinates (PDB code 5EWL) of NMDAR in complex with the non-covalent inhibitor MK-22 [19]. The ligands could be docked in the pocket thanks to a simulated induced fit procedure marginally modifying the side chain conformation of Tyr109 from the GluN1 subunit, given the structural difference between MK-22 and our compounds. Compounds **1**, **2** (Fig. 3) and **3** (Figure S5) bound consistently at the investigated pocket, adopting an orientation similar to the one displayed by the crystallographic compound. The galantamine substructure established H-bond interactions with the side chain of Arg115 of the GluN1 subunit and with the carboxylic group of Glu236 of the GluN2B subunit. It also established a hydrophobic interaction with the side chain of Phe176 of GluN2B. The protonated amine of the galantamine moiety

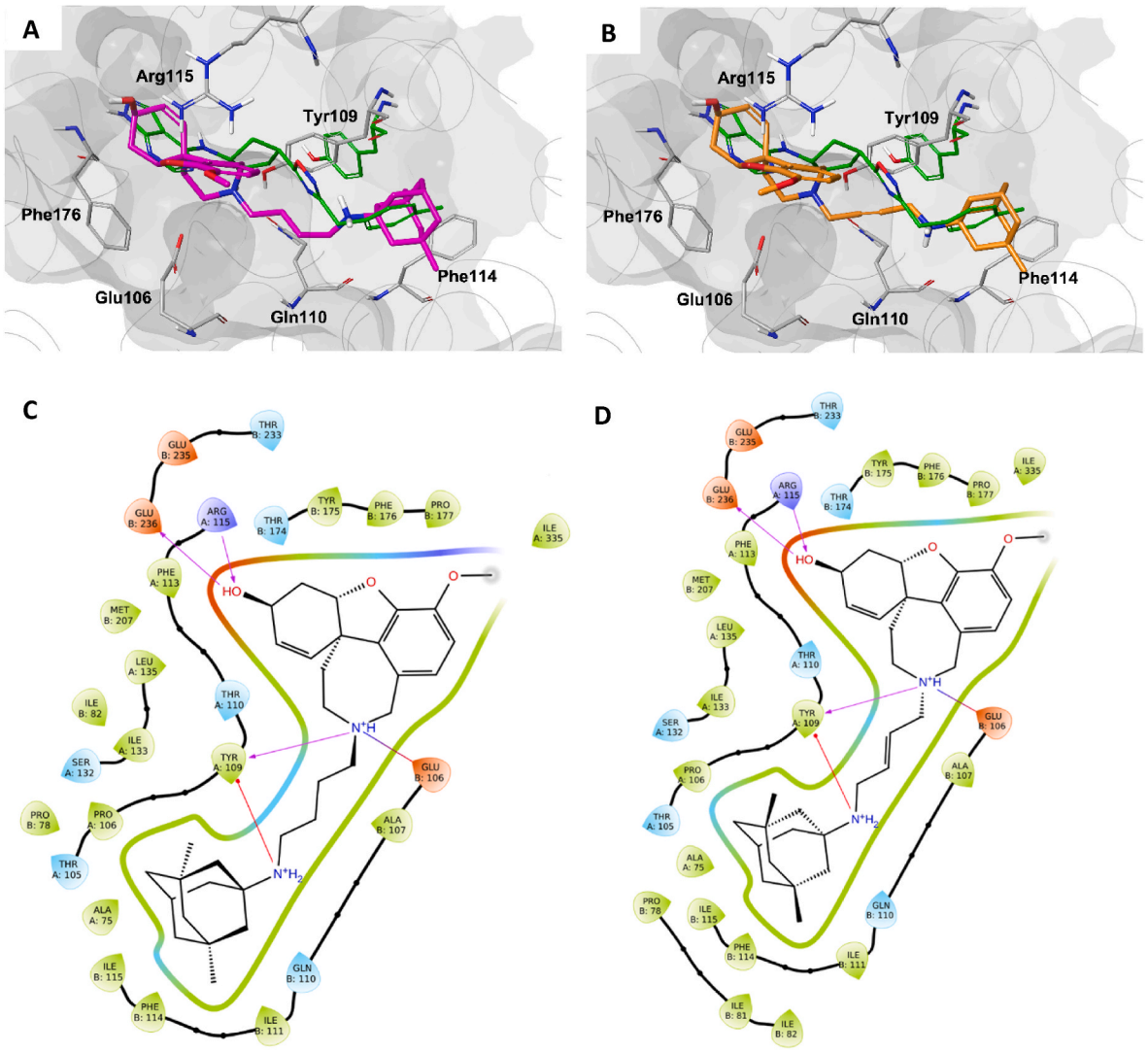

Fig. 3. Predicted bound conformation of compounds **1** (carbon atoms in magenta, A) and **2** (carbon atoms in orange, B) and protein-ligand interactions (*C*-D, respectively) at the MK-22 binding site described by the heterodimer formed by NMDA receptor subunits GluN1 and GluN2B. In panels A–B, the protein structure is reported in thin grey ribbon. Key residues of subunit GluN1 (Tyr109, and Arg115) and of subunit GluN2B (Glu106, Gln110, Phe114, and Phe176) are reported in stick representation with light grey carbons and labelled explicitly. The co-crystallised conformation of MK-22 is reported for reference (carbon atoms in green). The original orientation of the side chain of Tyr109 of GluN1 subunit before applying the induced fit docking protocol is reported in green. A grey mesh highlights the boundaries of the binding pocket. In panels *C*–D, all residues within 4 Å from the ligand are reported explicitly. Key protein-ligand interactions are depicted as follows: hydrogen bond, purple arrow; salt bridges, red-blue line; π – cation interaction, red circle; solvent exposed atoms are circled in grey.

Table 2
In vitro pharmacokinetic and metabolic characterization of compounds 1–3.

Cpd	Kinetic Solubility in PBS (μM)	Mouse Plasma Stability (min)[a]	Mouse Phase I Microsomal Stability (min)[b]	Mouse Phase II Microsomal Stability (min)[c]
1	242 ± 5	$t_{½} = 97$	$t_{½} > 60$	$t_{½} > 60$
2	237 ± 7	$t_{½} > 120$	$t_{½} = 45$	$t_{½} > 60$
3	230 ± 4	$t_{½} > 120$	$t_{½} < 5$	n.d.

n.d. = not determined.
[a] 2 μM of test compound was incubated at 37 °C for 2 h with mouse plasma (0.5% DMSO) and analyzed by LC-MS/MS at different time points.
[b] 5 μM of test compound was incubated at 37 °C for 1 h with mouse liver microsomes and the cofactors (NADPH, G6P, G6PDH and $MgCl_2$) in 0.1 M Tris-HCl buffer (pH 7.5) (0.1% DMSO) and analyzed by LC-MS/MS.
[c] 5 μM of test compound was incubated at 37 °C for 1 h with mouse liver microsomes, alamethicin and the cofactors (UDPGA, D-saccharic acid lactone and $MgCl_2$) in 0.1 M Tris-HCl buffer (pH 7.5) (0.1% DMSO) and analyzed by LC-MS/MS.

established a Coulombic interaction with the carboxylate group of Glu106 of GluN2B and donated an H-bond with the side chain of Tyr109 of GluN1. The linker was docked in a narrow hydrophobic cavity defined by Tyr109 and Phe113 of GluN1 and Pro78, Gln110, and Ile111 of GluN2B. The adamantane moiety formed a hydrophobic interaction with the aromatic ring of Phe114 of GluN2B while its charged amine established a π – cation interaction with the side chain of Tyr109 of GluN1.

The selectivity of compounds **1** and **2** for GluN1/2B over GluN1/2A can only be partially elucidated by the current docking model, in which protein flexibility is only considered in a very limited fashion. The sequence homology between GluN2B and GluN2A stands at 59.6%. Moreover, no significant distinctions could be detected among residues within 6 Å of the predicted binding sites, with only conservative substitutions observed (e.g., Ile81 and Thr233 in GluN2B correspond to Leu82 and Ser232 in GluN2A). However, we posit that subtle sequence variations in helices α1 and α2 (e.g., Ile111 in GluN2B versus Met112 in GluN2A) may induce minor structural adjustments. These helices constitute secondary structure elements that define the adaptable region that our model places in proximity to the memantine motif in our compounds. It is conceivable that compounds **1** and **2** exploit these local distinctions to achieve a more favorable fit within the GluN2B pocket, thereby accounting for their heightened affinity. Conversely, this possibility is ruled out for the less flexible compound **3**.

2.4. *In vitro pharmacokinetics*

Early pharmacokinetic characterization is becoming essential in drug discovery campaigns to possibly boost only efficient *in vivo* translation while avoiding unnecessary animal testing [20]. In pursuing drug-like properties, we first evaluated the effect of reduced linker flexibility in the pharmacokinetic and metabolic profiles of compounds **2** and **3** compared to **1** at *in vitro* level (Table 2).

Satisfactory solubility in aqueous neutral buffer was verified for compounds **1**–**3**. Then, compound stability (reported as half-life, $t_{½}$) under different experimental conditions was assessed by analysing the prepared incubation mixtures with a liquid chromatography - tandem mass spectrometry (LC-MS/MS) method at different time points. In murine plasma all tested chimeras proved to be stable, with compounds **2** and **3** also demonstrating an increase in stability compared to compound **1** ($t_{½}$ >120 *vs* 97 min). Furthermore, stability assays with murine liver microsomes were conducted to preliminarily evaluate the *in vivo* metabolic profile [21]. Particularly, by adding the appropriate cofactors (e.g., oxidating or conjugating enzymes) in the incubation mixture these assays can provide a reliable model of Phase I or II metabolism. Under Phase I conditions compound **3** underwent a fast degradation, precluding its further biological characterization. In the same experiment, compound **2** demonstrated a slightly reduced stability compared to compound **1** ($t_{½}$ = 45 *vs* > 60 min), but still feasible for *in vivo* administration. The introduction of an unsaturated fragment, with the aim to increase the brain exposure, clearly impacted on Phase I metabolism, albeit to a different extent for **2** and **3**, due to the different reactivity of the linker portion. Alkenes and alkynes are much more likely to undergo oxidation than alkanes thanks to their π-electrons and this could be the reason of the lower Phase I stability of new compounds [22]. Finally, both compounds **1** and **2** were completely stable under Phase II conditions and, given the results of all these *in vitro* analyses, were selected for *in vivo* PK examination.

2.5. *In vivo pharmacokinetics*

Based on its biological characterization, with improved biochemical profile and preliminary *in vitro* ADME properties, hybrid **2** was further evaluated *in vivo* and compared with parent compound **1**. Particularly, the formulations of compounds **1** and **2** in PEG400/Tween 80/Saline solution at 10/10/80% in volume respectively, were intravenously injected in male CD1 mice, weighing 22–24 g, at a dose of 3 mg/kg. Their plasma and brain concentrations were monitored at different time points (from 0.5 to 240 min after administration) allowing to define the key pharmacokinetic parameters (Fig. 4 and Tables 3 and 4). Three animals per each time point were treated.

The I.V. administration allows an immediate entrance in the bloodstream, justifying the similar maximal plasma concentration reached after only 5 min post injection for both compounds. The two compounds also share an almost equivalent plasmatic profile over time as confirmed by the respective AUC values. The half-life is lower while the clearance rate is higher for compound **2** in respect to compound **1**. Particularly, the half-life of compound **2** was 82 min in circulation (vs 1247 min for compound **1**) with the same compound still being present after 240 min post dosing. Moreover, compound **2** displayed a reduced volume of distribution demonstrating a suboptimal capability to distribute out of the circulating plasma compartment. Considered together, these results

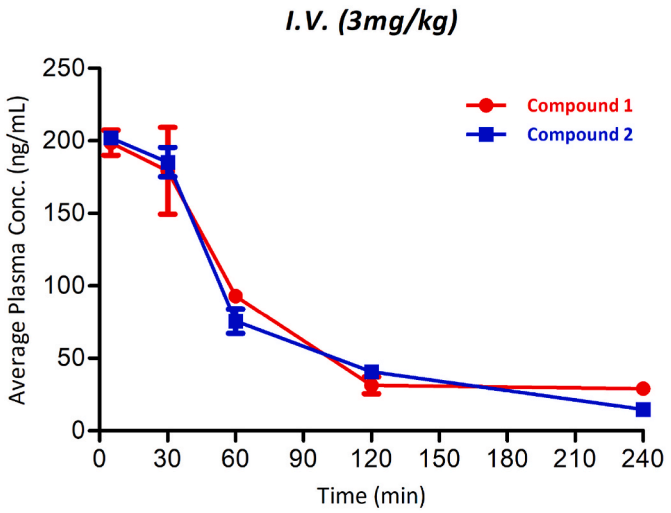

Fig. 4. Pharmacokinetic profiles of compounds **1** and **2** in mouse plasma. Strain: CD1. Route of administration: I.V. Dose: 3 mg/kg.

Table 3
Pharmacokinetic parameters of compounds 1 and 2.[a]

Parameter	Unit	Compound 1	Compound 2
C_{max}	ng/mL	208	202
t_{max}	min	5	5
AUC	min*ng/mL	17,378	16,802
$t_{½}$	min	1247	82
VD	L/kg	78	19
CL	mL/min/kg	43	161

[a] Maximum plasma concentration (C_{max}); time to reach maximum concentration (t_{max}); area under the curve (AUC); half-life ($t_{1/2}$); volume of distribution (VD); and clearance (CL).

Table 4
Brain profile of Compounds 1 and 2.

Time Point	Sample ID	Compound 1		Compound 2	
min		ng/mg Brain[a]	STD	ng/mg Brain[a]	STD
Vehicle	A_Veh B_Veh	**0**	0	**0**	0
5	A_5 B_5 C_5	**0.141**	0.093	**0.524**	0.461
30	A_30 B_30 C_30	**0.095**	0.084	**0.281**	0.222
60	A_60 B_60 C_60	**0.115**	0.077	**0.256**	0.444
120	A_120 B_120 C_120	**0.070**	0.121	**0.243**	0.229
240	A_240 B_240 C_240	**0.031**	0.054	**0.096**	0.167

Mouse strain: CD1; **Vehicle**: 10% TWEEN80 + 10% PEG400 in Saline; **Administration:** I.V. (3 mg/kg).
[a] Normalized by 100 mg brain/mL.

highlight a faster metabolism for compound **2**, in concordance with its lower *in vitro* Phase I microsomal stability (45 min compared with >60 min).

Finally, the brain uptake of compounds **1** and **2** was evaluated. As reported in Table 4, both compounds were able to rapidly permeate the brain in low quantity. Interestingly, however, compound **2** registered an improved brain permeation as determined by comparing the compound concentration at the t_{max}. Indeed, at t_{max} the average amount of **2** in the brain is more than 2 times the amount of **1**.

Although the brain exposure remains low, the improvement achieved with minimal structural modification was significant. The structural stiffening of the linker slightly ameliorates the overall physicochemical properties (Table 5). Besides rotatable bond reduction, by increasing the unsaturation grade, the pKa of the most basic center (i.e., memantine's nitrogen) decreases with a resulting higher cLogD value, approaching the optimal physicochemical properties for a successful CNS drug [8,23]. Notwithstanding, some pharmacokinetic drawbacks were encountered, which deserve further investigations. Particularly, a detailed metabolite analysis on compound **2** could be helpful to guide toward subsequent PK optimization.

3. Conclusion

Extensive neuronal death and cerebral atrophy resulting from the dysfunction of neurotransmitter systems represent morphological features of AD brain. Particularly, the cholinergic deficit and glutamate-mediated excitotoxicity are strictly related to the onset and development of characteristic cognitive decline. To date the standard of care treatment for AD still remains the co-administration of an AChE inhibitor with the NMDAR antagonist memantine, albeit with mainly symptomatic effects. Based on these premises, we previously developed a series of chimeric compounds by chemically combining the two marketed drugs memantine and galantamine in search of more efficient therapies. Among the new chimeras, compound **1** was able to modulate both NMDAR and AChE in the low micromolar range and demonstrated a promising neuroprotective profile both *in vitro* and *in vivo*, although a suboptimal PK profile required an undesirable i.c.v. administration. In this work we reduced the molecular flexibility of **1** in terms of rotatable bonds, which usually complicates brain penetration rate. Particularly, in compounds **2** and **3** the two pharmacophoric portions and linker length were left untouched while a double or triple bond was respectively inserted in the polymethylene bridge. Firstly, concerning compound **2**, this strategy paid off in terms of upgrading ChEs inhibition and NMDAR GluN1/2B selective antagonism. Indeed, the specific orientation of the alkene tether has enabled to reach submicromolar inhibition of both AChE and BChE (IC_{50} = 0.115 μM and 0.421 μM, respectively), and preferentially antagonize excitotoxicity-related GluN1/2B NMDAR over beneficial synaptic GluN1/2A NMDAR (IC_{50} = 1.32 *vs* 14.5 μM, SI = ~11). Conversely, the rigidity of the triple bond in the linker portion of **3** led to reduced NMDAR antagonism and ChE inhibitory effects. Both compounds showed an increased plasma stability with a different metabolic profile, relative to **1**. Fast degradation occurred for compound **3** in Phase I microsomal stability probably due to quicker oxidation at the alkyne moiety, avoiding its further biological investigation. Satisfactory stability in Phase I associated to a complete stability in Phase II metabolic condition made compound **2** suitable for subsequent *in vivo* PK evaluation. Intravenous administration of compound **2** in CD1 mice revealed a similar PK profile to **1** but highlighting a lower half-life and faster clearance. Finally, although the brain uptake remains low for a CNS-targeted drug, the brain permeation observed for compound **2** was higher in comparison to the parent compound. Thus, by reducing rotatable bond count in the linker portion, promising improvements were made from the pharmacological and pharmacokinetic point of view, representing the starting point for further chemical optimizations and *in vivo* biological investigations.

Table 5
Physicochemical parameters of compounds 1–3 compared to drugs memantine and galantamine.[a]

	Memantine	Galantamine	Compound 1	Compound 2	Compound 3	Optimal Physicochemical properties for CNS drug[b]
cLogP	2.07	1.16	4.07	4.02	3.96	2<cLogP<4
cLogD	−0.78	−0.04	−0.96	0.24	1.15	2<cLogD<3
MW	179.30	287.35	506.72	504.70	502.69	<450
TPSA	26.02	41.93	53.96	53.96	53.96	<90
HBD	1	1	2	2	2	<3
HBA	1	4	5	5	5	<7
pKa	10.70	8.58	11.18	10.34	9.75	6 < pKa<10.5
Num. rotatable bonds	0	1	7	6	4	<8
CNS MPO score	3.80	5.46	2.97	2.99	3.14	>4

[a] Properties computed by MarvinSketch21.3 and SwissADME (Sci. Rep. 2017, 7:42,717).
[b] Data taken from *J. Med. Chem*. 2021, 64, 18, 13,152–13173; *J. Med. Chem*. 2015, 58, 2584−2608; *ACS Chem. Neurosci*. 2016, 7, 767−775.

4. Material and methods

4.1. Chemistry

Chemical reagents were purchased from Merck, TCI and Fluorochem. *N*-Desmethylgalantamine was purchased from Synfine research. Nuclear magnetic resonance spectra (NMR) were recorded at 400 MHz for ^{1}H and 100 MHz for ^{13}C on Varian VXR 400 spectrometer in $CDCl_3$, DMSO-d_6 or CD_3OD as solvents. Chemical shifts (δ) are given in ppm from tetramethylsilane (TMS) with the solvent resonance as internal standard ($CDCl_3$: δ 7.26, DMSO-d_6: δ 2.50, CD_3OD: δ 3.31 for ^{1}H NMR and $CDCl_3$: δ 77.16, DMSO-d_6: δ 39.52, CD_3OD: δ 49.00 for ^{13}C NMR). For ^{1}H NMR, data are reported as follows: chemical shift, multiplicity (s = singlet, d = doublet, dd = double of doublets, t = triplet, q = quartet, m = multiplet, p = pentet, dt = doublet of triplets, td = triplet of doublets, tt = triplet of triplets, qd = quartet of doublets, br s = broad singlet), coupling constants (Hz) and integration. Chromatographic separations were performed on silica gel columns by flash or gravity column (Kieselgel 40, 0.040–0.063 mm; Merck) chromatography. Reactions were followed by thin-layer chromatography (TLC) on Merck (0.25 mm) glass-packed pre-coated silica gel plates (60 F^{254}) that were visualized in an iodine chamber, or with a UV lamp, $KMnO_4$, or bromocresol green. All the names were attributed by Chem BioDraw Ultra 21.0.0. For microwave-assisted reactions we used the microwave system for organic chemistry CEM Discover® SP (2.45 GHz, maximum potency 300 W). Optical rotations were measured on an Autopol II Automatic polarimeter using a sodium lamp (589 nm) as the light source; concentrations expressed in g/100 mL using $CHCl_3$ as a solvent and a 1 dm cell. All final compounds were analyzed by LC-MS starting from a 10 mM stock solution in DMSO-d_6 and further diluted 20-fold with CH_3CN–H_2O (1:1) for analysis. The analyses were performed on a Waters ACQUITY UPLC-MS system consisting of a single quadrupole detector (SQD) mass spectrometer equipped with an electrospray ionization (ESI) interface and a photodiode array detector (PDA) from Waters Inc. (Milford, MA, USA). The PDA range was 210–400 nm. ESI in positive mode was used in the mass scan range 100–650 Da. The analyses were run on an ACQUITY UPLC BEH C_{18} column (100 × 2.1 mmID, particle size 1.7 μm) with a VanGuard BEH C_{18} pre-column (5 × 2.1mmID, particle size 1.7 μm). The mobile phase was 10 mM NH_4OAc in H_2O at pH 5 adjusted with AcOH (A) and 10 mM NH_4OAc in CH_3CN–H_2O (95:5) at pH 5 (B) with 0.5 mL/min as flow rate. A linear gradient was applied: 0–0.2min: 10%B, 0.2–6.2min: 10–90%B, 6.2–6.3min: 90–100%, 6.3–7.0min: 100%B. All final compounds displayed a purity ≥95% as determined by UV at 215 nm. Accurate mass measurements (HRMS) was performed on a Waters Synapt G2 Q-ToF mass spectrometer equipped with an electrospray ionization interface (ESI) in positive mode and coupled to a Waters ACQUITY UPLC. Leucine Enkephalin (2 ng/mL) was used as lock mass reference compound for spectral recalibration. The analyses were run on an ACQUITY UPLC BEH C_{18} column (50 × 2.1 mmID, particle size 1.7 μm), using H_2O + 0.1% HCOOH (A) and CH_3CN + 0.1% HCOOH as mobile phase. Compound **1** was prepared as reported in Ref. [5].

4.2. Synthesis of compounds

4.2.1. Methyl (E)-4-[(3,5-dimethyladamantan-1-yl)amino]but-2-enoate (4)

Methyl-4-bromocrotonate (0.49 mL, 4.18 mmol) was added dropwise to a solution of 3,5-dimethyl-1-adamantanamine (500 mg, 2.79 mmol) and K_2CO_3 (963.95 mg, 6.98 mmol) in DMF (4 mL) and the reaction mixture was stirred vigorously under microwave irradiation (250 psi, 80 W) at 60 °C for 10 min. After evaporation of the solvent, the crude product was purified through column chromatography using DCM/methanol/ammonia water solution 33% (9.5/0.5/0.03) as mobile phase. Compound **4** was obtained as orange oil, 480 mg (62%). ^{1}H NMR ($CDCl_3$, 400 MHz) δ 7.01 (dt, ^{1}J = 15.6 Hz, ^{2}J = 6 Hz, 1H), 5.97 (d, J = 15.6 Hz, 1H), 3.70 (s, 3H), 3.38 (dd, ^{1}J = 6 Hz, ^{2}J = 2 Hz, 2H), 2.12–2.11 (m, 1H), 1.45–1.44 (m, 2H), 1.27–1.19 (m, 8H), 1.10–1.08 (m, 2H), 0.82 (s, 6H). ^{13}C NMR ($CDCl_3$, 100 MHz) δ 166.99, 148.33, 120.62, 52.58, 51.49, 50.90 (2C), 48.96 (2C), 42.95 (2C), 41.94, 41.26, 32.45 (2C), 30.29, 30.27.

4.2.2. Methyl (E)-4-[(tert-butoxycarbonyl) (3,5-dimethyladamantan-1-yl) amino]but-2-enoate (5)

Di-*tert*-butyldicarbonate (1.51 g, 6.92 mmol) and Na_2CO_3 (274.5 mg, 2.59 mmol) were added to a solution of **4** (480 mg, 1.73 mmol) in a THF/H_2O mixture 2:1 (4.5 mL) and the reaction mixture was stirred vigorously under microwave irradiation (250 psi, 80 W) at 60 °C for 2 h. After evaporation of the solvent under reduced pressure, the crude product was purified through flash column chromatography using petroleum ether/ethyl acetate (9/1) as mobile phase. Compound **5** was obtained as colourless oil, 570 mg (87%). ^{1}H NMR ($CDCl_3$,400 MHz) δ 6.85 (dt, ^{1}J = 16 Hz, ^{2}J = 4.2 Hz, 1H), 5.82 (d, J = 16 Hz, 1H), 4.03 (d, J = 4.2 Hz, 2H), 3.69 (s, 3H), 2.09–2.08 (m, 1H), 1.88–1.87 (m, 2H), 1.68 (s, 3H), 1.38 (s, 9H), 1.31–1.28 (m, 2H), 1.21–1.18 (m, 3H), 1.07–1.06 (m, 2H), 0.79 (s, 6H). ^{13}C NMR ($CDCl_3$, 100 MHz) δ 166.88, 154.81, 147.89, 120.36, 79.67, 58.56, 51.48, 50.39, 46.78, 44.50 (2C), 42.51 (2C), 39.28, 32.84 (2C), 30.62, 30.37 (2C), 28.45 (3C).

4.2.3. tert-butyl (3,5-dimethyladamantan-1-yl)[(E)-4-hydroxybut-2-en-1-yl]carbamate (6)

DIBAL-H 1 M in cyclohexane (3.77 mL, 3.77 mmol) was added to a solution of **5** (570 mg, 1.51 mmol) in THF (33 mL) at −78 °C under inert condition. After 4 h under stirring in these conditions 24 mL of ethyl acetate was added. Once the reaction mixture reached room temperature 24 mL of aqueous solution of tartaric acid 25% was added and left stirring for 20 min. The organic phase was separated and the aqueous one was further extracted with ethyl acetate (2 × 24 mL). Organic phases, once reunited, were washed sequentially with HCl 0.5 N (1 × 24 mL), $NaHCO_3$ 0.5 N (1 × 24 mL) and saturated aqueous solution of NaCl (1 × 24 mL). Organic extracts were dried with anhydrous Na_2SO_4 and, once evaporated the solvent under reduced pressure, compound **6** was obtained as colourless oil, 530 mg (99%). ^{1}H NMR ($CDCl_3$, 400 MHz) δ 5.69–5.67 (m, 2H), 4.14–4.13 (m, 2H), 3.93–3.92 (m, 2H), 2.13–2.12 (m, 1H), 1.94–1.93 (m, 2H), 1.74 (s, 3H), 1.44 (s, 9H),1.36–1.26 (m, 5H), 1.12–1.11 (m, 2H), 0.84 (s, 6H). ^{13}C NMR ($CDCl_3$, 100 MHz) δ 155.33, 131.19, 129.48, 79.42, 63.38, 58.59, 50.61, 47.02 (2C), 44.87, 42.75 (2C), 39.49, 32.94, 30.81 (2C), 30.57 (2C), 28.70 (3C).

4.2.4. tert-butyl [(E)-4-chlorobut-2-en-1-yl](3,5-dimethyladamantan-1-yl) carbamate (7)

Triphenylphosphine (194 mg, 0.74 mmol) was added gradually to a solution of **6** (130 mg, 0.37 mmol) in DCM (6 mL) at 0 °C, followed by the addition of *N*-chlorosuccinimide (74 mg, 0.56 mmol) and left stirring for 15 min at the same temperature. After evaporation of the solvent under reduced pressure, the obtained crude was purified through column chromatography using petroleum ether/ethyl acetate (9.5/0.5) as mobile phase. Compound **7** was obtained as colourless oil, 80 mg (60%). ^{1}H NMR ($CDCl_3$, 400 MHz) δ 5.71–5.68 (m, 2H), 4.06–4.04 (m, 2H), 3.93–3.92 (m, 2H), 2.13–2.12 (m, 1H), 1.93–1.92 (m, 2H), 1.73 (s, 3H), 1.44 (s, 9H), 1.35–1.20 (m, 5H), 1.12–1.10 (m, 2H), 0.83 (s, 6H). ^{13}C NMR ($CDCl_3$, 100 MHz) δ 155.18, 134.36, 126.42, 79.53, 58.69, 50.62, 47.00 (2C), 45.05, 44.68, 42.77 (2C), 39.49, 33.00 (2C), 30.86, 30.62 (2C), 28.69 (3C).

4.2.5. tert-butyl (3,5-dimethyladamantan-1-yl){(E)-4-[6-hydroxy-3-methoxy-4a,5,9,10-tetrahydro-6H-benzo[2,3]benzofuro[4,3-cd]azepin-11 (12H)-yl]but-2-en-1-yl}carbamate (8)

Triethylamine (50 μL, 0.35 mmol) and *N*-desmethyl-galantamine (48.4 mg, 0.18 mmol) were added to a solution of **7** (65 mg, 0.18 mmol) in acetonitrile (2 mL) and the reaction mixture was left stirring at 75 °C in pressure tube (Ace pressure tubes-Sigma Aldrich). After 7 h, solvent was evaporated under reduced pressure and the obtained crude product

was purified through column chromatography using DCM/methanol (9/1) as mobile phase. Compound **8** was obtained as colourless oil, 75 mg (70%). ^{1}H NMR ($CDCl_3$, 400 MHz) δ 6.61 (dd, ^1J = 20 Hz, ^2J = 8 Hz, 2H), 6.06 (d, J = 8 Hz, 1H), 6.00 (dd, ^1J = 12 Hz, ^2J = 8 Hz, 1H) 5.57–5.53 (m, 2H), 4.61 (br s, 1H), 4.12–4.08 (m, 2H), 3.92–3.86 (m, 2H), 3.82 (s, 3H), 3.32–3.15 (m, 3H), 2.68 (d, J = 16 Hz, 1H), 2.13–2.12 (m, 1H), 2.02–1.95 (m, 4H), 1.78–1.71 (m, 4H), 1.56–1.55 (m, 2H), 1.45 (s, 9H), 1.34–1.21 (m, 6H), 1.11 (s, 2H), 0.83 (s, 6H). ^{13}C NMR ($CDCl_3$, 100 MHz) δ 155.23, 145.80, 143.98, 133.37, 132.77, 129.37, 128.55, 127.52, 126.96, 122.40, 111.47, 88.87, 79.35, 62.20 (2C), 58.60, 56.08, 51.50, 50.68, 48.47, 47.08 (2C), 45.10 (2C), 42.83 (2C), 39.55, 32.98, 30.87, 30.65 (2C), 30.12, 28.79 (5C).

4.2.6. 11-{(E)-4-[(3,5-dimethyladamantan-1-yl)amino]-but-2-en-1-yl}-3-methoxy-4a, 5,9,10,11,12-hexahydro-6H-benzo[2,3]benzofuro[4,3-cd] azepin-6-ol (2)

HCl 4 M in dioxane (3 mL) was added dropwise to compound **8** (75 mg, 0.12 mmol) at 0 °C and the reaction mixture was vigorously stirred for 50 min at the same temperature. After solvent evaporation under reduced pressure, the obtained crude product was purified through column chromatography using DCM/methanol/aqueous ammonia solution 33% (9/1/0.1) as mobile phase. Compound **2** was obtained as colourless oil, 40 mg (63%). ^{1}H NMR (DMSO-d_6, 400 MHz) δ 6.69 (d, J = 8 Hz, 1H), 6.52 (d, J = 8 Hz, 1H), 6.08 (d, J = 12 Hz, 1H), 5.80 (dd, ^1J = 12 Hz, ^2J = 4 Hz, 1H), 5.55–5.48 (m, 2H), 4.48 (br s, 1H), 4.20 (br s, 1H), 4.08–4.04 (m, 2H), 3.69–3.65 (m, 1H), 3.73 (s, 3H), 3.18–3.17 (m, 3H), 3.03–2.8 (m, 3H), 2.27–2.23 (m, 1H), 2.09–1.93 (m, 3H), 1.44 (s, 2H), 1.34 (s, 1H), 1.28–1.20 (m, 8H), 1.12–1.04 (m, 2H), 0.82 (s, 6H). ^{13}C NMR ($CDCl_3$, 100 MHz) δ 145.79, 143.96, 133.14, 132.76, 129.36, 128.53, 127.50, 126.94, 121.96, 111.19, 88.61, 61.98, 57.99, 55.84, 55.05, 52.62, 51.50, 50.84 (2C), 48.79, 48.25, 42.89 (2C), 42.68, 41.10, 33.76, 32.34, 30.23 (2C), 30.20 (2C), 29.91. $[\alpha]_D^{29.2} = -37.143 \pm 0.039$ (c 0.05, $CHCl_3$). UV purity (215 nm): 97%, HRMS (ESI+) calcd for $C_{32}H_{44}N_2O_3$ $[M+H]^+$ 505.3425, found 505.4329.

4.2.7. 4-[(tert-butyldimethylsilyl)oxy]but-2-yn-1-ol (9)

Triethylamine (0.97 mL, 6.98 mmol) and a solution of *tert*-butyldimethylsilyl chloride (TBDMSCl) (700.9 mg, 4.65 mmol) in DCM (4 mL) were added through dropping funnel over 30 min at 0 °C to 2-butyne-1,4-diol (1 g, 11.62 mmol) in DMF (4 mL). The reaction mixture was stirred for 18 h at room temperature. After solvent evaporation under reduced pressure, the obtained crude product was purified through column chromatography using petroleum ether/ethyl acetate (6/4) as mobile phase. Compound **9** was obtained as colourless oil, 620 mg (67%). ^{1}H NMR ($CDCl_3$, 400 MHz) δ 4.27 (s, 2H), 4.20 (s, 2H), 0.84 (s, 9H), 0.05 (s, 6H). ^{13}C NMR ($CDCl_3$, 100 MHz) δ 83.79, 83.34, 51.68, 50.66, 25.74 (3C), 18.21, −5.28 (2C).

4.2.8. 4-([tert-butyldimethylsilyl)oxy]but-2-yn-1-yl 4-methylbenzensulfonate (10)

Triethylamine (1.3 mL, 9.3 mmol), tosyl chloride (709.22 mg, 3.72 mmol) and dimethylaminopyridine (cat. amount) were added to a solution of **9** (620 mg, 3.10 mmol) in DCM (6 mL) at 0 °C. After 10 min of stirring the solvent was evaporated under reduced pressure and the obtained crude product was purified through flash column chromatography using petroleum ether/ethyl acetate (9/1) as mobile phase. Compound **10** was obtained as colourless oil, 270 mg (25%). ^{1}H NMR ($CDCl_3$, 400 MHz) δ 7.78 (d, J = 8 Hz, 2H), 7.31 (d, J = 8 Hz, 2H), 4.70 (s, 2H), 4.18 (s, 2H), 2.42 (s, 3H), 0.85 (s, 9H), 0.04 (s, 6H). ^{13}C NMR ($CDCl_3$, 100 MHz) δ 144.99, 133.09, 129.78 (2C), 128.08 (2C), 88.04 (2C), 57.97, 51.41, 25.71 (3C), 21.62, 18.20, −5.30 (2C).

4.2.9. N-{4-[(tert-butyldimethylsilyl)oxy]but-2-yn-1-yl}-3,5-dimethyladamantan-1-amine (11)

3,5-Dimethyl-1-adamantanamine (136.6 mg, 0.76 mmol) and K_2CO_3 (263.3 mg, 1.91 mmol) were added to a solution of **10** (270 mg, 0.76 mmol) in DMF (5 mL) and the reaction mixture was stirred vigorously under microwave irradiation (250 psi, 80 W) at 80 °C for 20 min. After evaporation of the solvent under reduced pressure, the obtained crude product was purified through flash column chromatography using DCM/methanol/aqueous ammonia solution 33% (9.5/0.5/0.05) as mobile phase. Compound **11** was obtained as yellowish oil, 250 mg (91%). ^{1}H NMR ($CDCl_3$, 400 MHz) δ 4.29 (s, 2H), 3.43 (s, 2H), 2.11–2.10 (m, 1H), 1.49–1.48 (m, 2H), 1.31–1.24 (m, 8H), 1.10–1.08 (m, 3H), 0.89 (s, 9H), 0.82 (s, 6H), 0.09 (s, 6H). ^{13}C NMR ($CDCl_3$, 100 MHz) δ 83.85, 81.25, 51.92, 50.77, 48.49 (2C), 42.82 (3C), 40.86, 32.38 (2C), 30.57, 30.24 (2C), 30.16, 25.84 (3C), 25.77, −5.17 (2C).

4.2.10. tert-butyl {4-[(tert-butyldimethylsilyl)oxy]but-2-yn-1-yl}(3,5-dimethyladamantan-1-yl)carbamate (12)

Di-*tert*-butyldicarbonate (507 mg, 2.32 mmol) and Na_2CO_3 (123 mg, 1.16 mmol) were added to a solution of **11** (280 mg, 0.77 mmol) in a THF/H_2O mixture 2:1 (2.1 mL) and the reaction mixture was stirred vigorously under microwave irradiation (250 psi, 80 W) at 60 °C for 2 h. After evaporation of the solvent under reduced pressure, the crude product was purified through flash column chromatography using petroleum ether/ethyl acetate (9.5/0.5) as mobile phase. Compound **12** was obtained as colourless oil, 180 mg (50%). ^{1}H NMR ($CDCl_3$, 400 MHz) δ 4.25 (s, 2H), 4.03 (s, 2H), 2.09–2.08 (m, 1H), 1.97–1.96 (m, 2H), 1.79–1.72 (m, 4H), 1.40 (s, 9H), 1.32–1.29 (m, 2H), 1.21–1.18 (m, 2H), 1.08–1.06 (m, 2H), 0.84 (s, 9H), 0.79 (s, 6H), 0.06 (s, 6H). ^{13}C NMR ($CDCl_3$, 100 MHz) δ 154.92, 85.05, 80.19, 79.74, 58.64, 51.85, 50.53, 46.54 (2C), 42.64 (2C), 38.99, 33.25, 30.70, 30.48 (2C), 28.54 (3C), 27.42 (2C), 25.86 (3C), 18.27, −4.99 (2C).

4.2.11. tert-butyl (3,5-dimethyladamantan-1-yl) (4-hydroxybut-2-yn-1-yl) carbamate (13)

Tetra-*N*-butylammonium fluoride (TBAF) 1 M in THF (0.56 mL, 1.95 mmol) was added dropwise to a solution of **12** (180 mg, 0.39 mmol) in THF (1 mL) and was left stirring for 30 min under inert atmosphere at room temperature. Aqueous saturated solution of ammonium chloride (3 mL) was added to quench the reaction. After 30 min stirring, extractions with ethyl acetate (3 × 10 mL) were performed and the organic phases, once reunited, were dried with anhydrous Na_2SO_4. After evaporation of the solvent under reduced pressure, the crude product was purified through flash column chromatography using petroleum ether/ethyl acetate (7/3) as mobile phase. Compound **13** was obtained as colourless oil, 120 mg (89%). ^{1}H NMR ($CDCl_3$, 400 MHz) δ 4.24 (s, 2H), 4.08 (s, 2H), 2.14–2.12 (m, 1H), 1.98–1.97 (m, 2H), 1.91 (br s, 1H), 1.81–1.74 (m, 4H), 1.45 (s, 9H), 1.35–1.32 (m, 2H), 1.25–1.23 (m, 2H), 1.15–1.07 (m, 2H), 0.83 (s, 6H). ^{13}C NMR ($CDCl_3$, 100 MHz) δ 155.30, 84.60, 80.14, 80.01, 58.84, 51.34, 50.59, 46.80 (2C), 42.71 (2C), 39.23, 33.34, 32.96 (2C), 30.79, 30.58 (2C), 28.66 (3C).

4.2.12. 4-[(tert-butoxycarbonyl) (3,5-dimethyladamantan-1-yl)amino] but-2-yn-1-yl 4-methylbenzensulfonate (14)

Triethylamine (0.15 mL, 1.05 mmol), tosyl chloride (80 mg, 0.42 mmol) and dimethylaminopyridine (cat. amount) were added at 0 °C to a solution of **13** (120 mg, 0.35 mmol) in DCM (2 mL) and the reaction mixture was left stirring 15 min at room temperature. Solvent was evaporated under reduced pressure and the obtained crude product was purified through flash column chromatography using petroleum ether/ethyl acetate (8/2) as mobile phase. Compound **14** was obtained as colourless oil, 80 mg (46%). ^{1}H NMR ($CDCl_3$, 400 MHz) δ 7.77 (d, J = 8.4 Hz, 2H), 7.31 (d, J = 8.4 Hz, 2H), 4.66 (s, 2H), 3.99 (s, 2H), 2.41 (s, 3H), 2.11–2.10 (m, 1H), 1.90–1.89 (m, 2H), 1.71 (s, 4H), 1.42 (s, 9H), 1.33–1.30 (m, 2H), 1.23–1.20 (m, 2H), 1.10–1.08 (m, 2H), 0.81 (s, 6H). ^{13}C NMR ($CDCl_3$, 100 MHz) δ 154.80, 144.89, 133.04, 129.75 (2C), 127.92 (2C), 88.28, 80.01, 73.45, 58.69, 58.11, 50.31, 46.49 (2C), 42.45 (2C), 38.98, 33.03, 32.76 (2C), 30.58, 30.33 (2C), 28.39 (3C), 21.57.

4.2.13. tert-butyl (3,5-dimethyladamantan-1-yl){4-[6-hydroxy-3-methoxy-4a, 5,9,10-tetrahydro-6H-benzo[2,3]benzofuro[4,3-cd]azepin-11 (12H)-yl]but-2-yn-1-yl}carbamate (15)

Triethylamine (40 μL, 0.32 mmol) and *N*-desmethyl-galantamine (43.5 mg, 0.16 mmol) were added to a solution of **14** (80 mg, 0.16 mmol) in acetonitrile (1 mL) and the reaction mixture was left stirring e at 75 °C in pressure tube (Ace pressure tubes-Sigma Aldrich). After 30 min, solvent was evaporated under reduced pressure and the obtained crude product was purified through column chromatography using DCM/methanol (9/1) as mobile phase. Compound **15** was obtained as yellowish oil, 30 mg (31%). ^{1}H NMR ($CDCl_3$, 400 MHz) δ 6.64 (s, 2H), 6.05 (d, $J = 10.2$ Hz, 1H), 5.99 (dd, $^1J = 10.2$ Hz, $^2J = 5$ Hz, 1H), 4.59 (br s, 1H), 4.14–4.10 (m, 3H), 3.81 (s, 3H), 3.43 (s, 2H), 3.34–3.19 (m, 2H), 2.67 (d, J = 15.2 Hz, 1H), 2.44–2.40 (m, 1H), 2.15–2.14 (m, 1H), 2.07–1.97 (m, 4H), 1.86–1.79 (m, 4H), 1.66–1.59 (m, 1H), 1.47 (s, 9H), 1.37–1.25 (m, 6H), 1.16–1.09 (m, 2H), 0.84 (s, 6H). ^{13}C NMR ($CDCl_3$, 100 MHz) δ 155.00, 145.94, 144.27, 132.98, 129.58, 127.78, 126.88, 122.16, 111.35, 88.72 (2C), 79.83 (2C), 62.04, 58.67, 58.49, 55.94, 51.67, 50.52, 48.13, 46.69 (2C), 44.96, 42.65 (2C), 39.14, 34.74, 33.31, 32.87 (2C), 30.71, 30.52 (2C), 29.94, 28.60 (3C).

4.2.14. 11-{4-[(3,5-dimethyladamantan-1-yl)amino]but-2-yn-1-yl}-3-methoxy-4a, 5,9,10,11,12-hexahydro-6H-benzo[2,3]benzofuro[4,3-cd] azepin-6-ol (3)

HCl 4 M in dioxane (1.7 mL) was added dropwise to compound **15** (30 mg, 0.05 mmol) at 0 °C and the reaction mixture was vigorously stirred for 40 min at the same temperature. After solvent evaporation under reduced pressure, the obtained crude product was purified through column chromatography using DCM/methanol/aqueous ammonia solution 33% (9/1/0.1) as mobile phase. Compound **3** was obtained as yellowish oil, 16 mg (63%). ^{1}H NMR ($CDCl_3$, 400 MHz) δ 6.64 (s, 2H), 6.06 (d, $J = 10.4$ Hz, 1H), 6.00 (dd, $^1J = 10.4$ Hz, $^2J = 4.8$ Hz, 1H), 4.59 (br s, 1H), 4.14–4.07 (m, 2H), 3.82 (s, 3H), 3.66–3.62 (m, 1H), 3.48 (s, 2H), 3.40 (s, 2H), 3.27–3.23 (m, 2H), 2.67 (d, $J = 15.6$ Hz, 1H), 2.15–2.14 (s, 1H), 2.03–1.95 (m, 2H), 1.65–1.61 (m, 1H), 1.55 (s, 2H), 1.47 (s, 1H), 1.37–1.25 (m, 9H), 1.15–1.07 (m, 2H), 0.84 (s, 6H). ^{13}C NMR ($CDCl_3$, 100 MHz) δ 145.93, 144.23, 133.10, 128.97, 127.71, 127.04, 122.18, 111.31, 88.79 (2C), 77.30, 62.14, 58.69, 55.99, 51.73, 50.80, 48.37, 48.24 (2C), 44.80, 42.84 (2C), 40.74, 34.70, 32.52 (2C), 30.63, 30.31 (2C), 30.25, 29.99, 29.78. $[\alpha]_D^{28.1} = -49.676 \pm 0.249$ (*c* 0.06, $CHCl_3$). UV purity (215 nm): 99%, HRMS (ESI+) calcd for $C_{32}H_{42}N_2O_3$ $[M+H]^+$ 503.3268, found 503.4155.

4.3. Cholinesterases inhibition analyses

Human recombinant AChE (E.C. 3.1.1.7) lyophilized powder and BChE (E.C. 3.1.1.8) from human serum were from Merck Millipore, Italia. The capacity of tested compounds to inhibit hAChE and hBChE activity was assessed by Ellman's method [9]. In brief, assays were performed at 37 °C with a Jasco V-530 double beam Spectrophotometer equipped with a thermostated cuvette holder. hAChE stock solution was prepared by dissolving human AChE lyophilized powder in 0.1 M phosphate buffer (pH = 8.0) containing Triton X-100 0.1%. Stock solution of human BChE was prepared by dissolving lyophilized powder in an aqueous solution of gelatine 0.1%. Stock solutions of inhibitors (2 mM) were prepared in methanol. Assay solution consisted of a 0.1 M phosphate buffer (pH = 8.0), with the addition of 340 μM Ellman's reagent (Merck Millipore), 0.02 unit/mL of either hAChE or hBChE and 550 μM of substrate (acetylthiocholine or butyrylthiocholine, respectively). Aliquots of increasing concentration of the tested compound were added to the assay solution and preincubated for 20 min at 37 °C in the presence of the enzyme, before the addition of substrate. The rate of reaction was calculated by continuously monitoring the increase in the absorbance at 412 nm for 3 min.

Assays were carried out with a blank containing all components except enzymes (AChE or BChE) in order to account for the non-enzymatic reaction. The reaction rates were compared and the percent inhibition due to the presence of tested inhibitor at increasing concentration was calculated. Each concentration was analyzed in triplicate, and IC_{50} values were determined graphically from log concentration–inhibition curves (GraphPad Prism 4.03 software, GraphPad Software Inc.). Each IC_{50} value was determined from at least two independent experiments.

4.4. NMDAR inhibition studies

pRK7 plasmids containing rat GluN1 (1a variant), GluN2A or GluN2B cDNA inserts were linearized and their cRNA transcribed using the message machine transcription kit (Ambion) according to the manufacturers instructions. Each cRNA concentration was adjusted to 200 ng/μL and they were stored at −80 °C.

Xenopus laevis oocytes were obtained as ovary tissue from the European Xenopus Resource Center (University of Portsmouth, UK). The ovary tissue was treated with 0.5 mg/mL collagenase Type 1 A (Sigma, UK) in Ca^{2+}-free modified Barth's saline (MBS) (96 mM NaCl, 2 mM KCl, 5 mM HEPES, 2.5 mM pyruvic acid, 0.5 mM theophylline, pH 7.5) for 1 h at 18 °C to release individual oocytes and to remove the follicular tissue surrounding the oocytes. The separated oocytes were washed with Ca^{2+}-free MBS a minimum of five times then placed in MBS (96 mM NaCl, 2 mM KCl, 1.8 mM $CaCl_2$, 5 mM HEPES, 2.5 mM pyruvic acid, 0.5 mM theophylline, 0.05 mg/mL gentamicin, pH 7.5) at 18 °C. Healthy stage IV-V oocytes were selected and each one was injected with 50 nL of cRNA containing a 1:1 mixture of either GluN1 + GluN2A or GluN1 + GluN2B cRNAs (each at 100 ng/μL) using a Nanoliter 2010 injector (World Precision Instruments, UK). Oocytes were incubated for 3–4 days at 18 °C prior to electrophysiological recordings.

Whole-cell current recordings were obtained from oocytes expressing NMDARs by two-electrode voltage clamp using an Axoclamp 2 A voltage clamp amplifier (Axon instruments, USA). Oocytes were individually placed in a perfusion chamber and perfused (~5 mL/min) with standard oocyte saline (95 mM NaCl, 2 mM KCl, 2 mM $CaCl_2$, 5 mM HEPES, pH 7.5). Microelectrodes were pulled from borosilicate glass capillaries (GC150TF-4, Harvard Apparatus, UK) using a programmable micropipette puller (P-97, Sutter Instruments Co., USA) and had resistances between 0.5 and 2.5 MΩ when filled with 3 M KCl. Each oocyte was voltage-clamped at a holding potential of −75 mV. Whole-cell currents were evoked by application of 100 μM NMDA plus 10 μM glycine, applied using a gravity fed multi-channel perfusion system (MPS-2, World Precision Instruments, UK). The inhibitory actions of compounds **1**–**3** and memantine were assessed by their co-application with 100 μM NMDA plus 10 μM glycine, at concentrations in the range of 0.01 μM–100 μM in 10-fold steps. Output currents were transferred to a Windows PC using an NI PCI-6221/BNC-2110 digital interface (National Instruments, USA) and WinEDR software (Dr John Dempster, Institute of Pharmacy & Biomedical Sciences, University of Strathclyde, UK) was used for recording.

Currents evoked by 100 μM NMDA plus 10 μM glycine were measured (WinEDR) at their steady state in the presence of **1**–**3** or memantine and normalized (%) to the current in their absence (control response). Mean % control response was plotted against log concentration of **1**–**3** or memantine and fitted with the following equation to determine their IC_{50} (half maximal inhibitory concentration) values:

$$\%\ control\ response = \frac{100}{1 + 10^{(logIC50 - log[I]) \times s}}$$

where *[I]* is the concentration of the inhibitor and *s* is the Hill slope. All data plotting and curve fitting was conducted using GraphPad Prism 8.

4.5. Docking studies

Ligand docking simulations were carried out using Glide as implemented in Schrödinger 2022–01 (Schrödinger LLC, New York, USA) [24]. For each docked pose, a schematic representation of protein-ligand interactions was generated using the 2D Workspace - Ligand Interaction Diagram function as implemented in Schrödinger (Schrödinger LLC, New York, USA). All the ligands were prepared using the LigPrep tool. Standard parameters were used. Docking studies at the binding site of AChE were performed using the crystal structure of human AChE solved in complex with donepezil (PDB code 4EY7). The donepezil-bound co-crystal was superimposed to the structure of the human enzyme solved in complex with galantamine (PDB code 4EY6) using the Schrödinger Protein Structure Alignment tool and the aligned coordinates of galantamine stored [11]. This superimposition was performed to use galantamine as a reference in predicting the binding pose of our compounds while retaining the donepezil-bound orientation of the side chains in the binding pocket. These are already adapted to lodge ligands concurrently contacting both the catalytic site and the peripheral anionic site. The receptor was prepared using the Protein Preparation tool implemented in Schrödinger 2022–01, using default parameters. The size of the outer binding box was set equal to 20 Å to accommodate our compounds while the position and size of the inner box were defined by the coordinates of donepezil. The standard Glide SP protocol was used for docking [25]. Each compound was docked scaling by a factor of 0.8 the van der Waals radii of all protein and ligand atoms with partial charges $\leq$0.15. The conformational sampling was biased toward matching within 0.1 Å of the coordinates of the maximum common substructure that exists between galantamine and the investigated ligands. For each ligand up to 5 poses were retained, which were subsequently minimized after docking.

Docking studies at the binding site of BChE were performed using the crystal structure of human BChE solved in complex with tacrine (PDB code 4BDS) [15]. The tacrine-bound co-crystal was superimposed to the structure of the human AChE enzyme solved in complex with galantamine (PDB code 4EY6) using the Schrödinger Protein Structure Alignment tool and the aligned coordinates of galantamine stored. This superimposition was performed to use galantamine as a reference in predicting the binding pose of our compounds. The receptor was prepared using the Protein Preparation tool implemented in Schrödinger 2022–01, using default parameters. The size of the outer binding box was set equal to 20 Å to accommodate our compounds while the position and size of the inner box were defined by the coordinates of tacrine. The standard Glide SP protocol was used for docking. Each compound was docked scaling by a factor of 0.8 the van der Waals radii of all protein and ligand atoms with partial charges $\leq$0.15. The conformational sampling was biased toward matching within 0.1 Å of the coordinates of the maximum common substructure that exists between galantamine and the investigated ligands. For each ligand up to 5 poses were retained, which were subsequently minimized after docking.

The coordinates of the dimer containing subunits GluN1 and GluN2B (PDB code 5EWL) [19] of the NMDA receptor in complex with the non-covalent inhibitor MK-22 were processed with the Protein Preparation routine. Defaults parameters were used. The coordinates of the co-crystallised ligand were used to define the position and the size of the inner binding box while the size of the outer binding box was set equal to 20 Å. Then, MK-22 was removed from the complex. Given the structural difference between the co-crystallised ligand and the investigated molecules an induced fit protocol (IFD) was adopted [26]. In the first step of the IFD protocol, each prepared ligand was docked scaling by a factor of 0.5 the van der Waals radii of all protein atoms with partial charges $\leq$0.15. The standard Glide SP protocol was used for the first round of posing. Up to 20 poses were retained and progressed to the next step. Each generated complex was refined using Prime [27]. All residues with at least one heavy atom within 5 Å from the ligand were optimised. Last, ligands were re-docked into structures within 30 kcal/mol from the top scoring one, and within the top 20 structures overall. Again, Glide SP protocol was used. For each ligand, the best pose was retained. All calculations were carried out using the OPLS4 force field [28].

4.6. In vitro physico-chemical and metabolic stability analyses

4.6.1. Aqueous kinetic solubility

The aqueous kinetic solubility was determined from a 10 mM DMSO stock solution of test compound in Phosphate Buffered Saline (PBS) at pH 7.4. The study was performed by incubation of an aliquot of 10 mM DMSO stock solution in PBS (pH 7.4) at a target concentration of 250 μM (2.5% DMSO). The incubation was carried out under shaking at 25 °C for 24 h followed by centrifugation at 21,100×*g* for 30 min. The supernatant was further diluted (4:1) with CH_3CN and analyzed by UPLC-MS for the quantification of dissolved compound (in μM) by UV at a specific wavelength (215 nm). The aqueous kinetic solubility (in μM) was calculated by dividing the peak area of the dissolved test compound (supernatant) by the peak area of the test compound in reference (250 μM in CH_3CN) and further multiplied by the target concentration and dilution factor. The UPLC-MS analyses were performed on a Waters ACQUITY UPLC-MS system consisting of a single quadrupole detector (SQD) mass spectrometer equipped with an electrospray ionization (ESI) interface and a photodiode array detector (PDA) from Waters Inc. (Milford, MA, USA). The PDA range was 210–400 nm. ESI in positive mode was used in the mass scan range 100–650 Da. The analyses were run on an ACQUITY UPLC BEH C_{18} column (50 × 2.1 mm ID, particle size 1.7 μm) with a VanGuard BEH C_{18} pre-column (5 × 2.1 mm ID, particle size 1.7 μm), using 10 mM NH_4OAc in H_2O at pH 5 adjusted with AcOH (A) and 10 mM NH_4OAc in CH_3CN–H_2O (95:5) at pH 5 (B) as mobile phase. Values are reported as mean values of $\geq$2 experiments performed.

4.6.2. Plasma stability study

10 mM DMSO stock solution of test compound was diluted 50-fold with DMSO-H_2O (1:1) and incubated at 37 °C for 2 h with mouse plasma containing 5% DMSO (pre-heated at 37 °C for 10min). The final compound concentration was 2 μM (0.5% DMSO). At each time point (0, 5, 15, 30, 60, 120 min), an aliquot of incubation mixture was diluted (1:3) with cold CH_3CN spiked with 200 nM of an appropriate internal standard, followed by centrifugation at 3.270×*g* for 20 min. The supernatant was further diluted (1:1) with H_2O and analyzed by LC-MS/MS on a Waters ACQUITY UPLC-MS/MS system consisting of a triple quadrupole detector (TQD) mass spectrometer equipped with an electrospray ionization interface (ESI) and a photodiode array λ detector (PDA) from Waters Inc. (Milford, MA, USA). Electrospray ionization was applied in positive mode. Compound-dependent parameters as MRM transitions and collision energy were developed for each compound. The analyses were run on an ACQUITY UPLC BEH C_{18} (50 × 2.1 mm ID, particle size 1.7 μm) with a VanGuard BEH C_{18} pre-column (5 × 2.1 mm ID, particle size 1.7 μm) at 40 °C, using H_2O + 0.1% HCOOH (A) and CH_3CN + 0.1% HCOOH (B) as mobile phase. The percentage of test compound remaining at each time point relative to t = 0 was calculated by the response factor on the basis of the internal standard peak area. The percentage of test compound versus time was plotted and fitted by GraphPad Prism (GraphPad Software, Version 5 for Windows, CA, USA, www.graphpad.com) to estimate the compound's half-life ($t_{½}$) which was reported as mean value along with the standard deviation ($n = 3$).

4.6.3. Microsomal stability study – phase I and II

Phase I: 10 mM DMSO stock solution of test compound was pre-incubated at 37 °C for 15 min with mouse liver microsomes in 0.1 M Tris-HCl buffer (pH 7.5) containing 10% DMSO. The final compound concentration was 5 μM (0.1% DMSO). After pre-incubation, the co-factors (NADPH, G6P, G6PDH and $MgCl_2$ pre-dissolved in 0.1 M Tris-HCl) were added to the incubation mixture and the incubation was continued at 37 °C for 1 h.

Phase II: 10 mM DMSO stock solution of test compound was pre-incubated at 37 °C for 15 min with mouse liver microsomes added alamethicin (10 mg/mL) in 0.1 M Tris-HCl buffer (pH 7.5) containing 10% DMSO. The final compound concentration was 5 μM (0.1% DMSO). After pre-incubation, the cofactors (UDPGA, D-saccharic acid lactone and $MgCl_2$ pre-dissolved in 0.1 M Tris-HCl) were added to the incubation mixture and the incubation was continued at 37 °C for 1 h.

For both *Phase I and II* studies: At each time point (0, 5, 15, 30, 60 min), 30 μL of incubation mixture was diluted with 200 μL cold CH_3CN spiked with 200 nM of an appropriate internal standard, followed by centrifugation at 3.270×*g* for 15 min. The supernatant was further diluted (1:1) with H_2O for analysis. A reference incubation mixture (microsomes *without* cofactors) was prepared for each test compound and analyzed at t = 0 and 60 min in order to verify the compound's stability in the matrix. The two time points were diluted as for the time points of the incubation mixture above. The supernatants were analyzed by LC-MS/MS on a Waters ACQUITY UPLC-MS/MS system as defined above. The percentage of test compound remaining at each time point relative to t = 0 was calculated by the response factor on the basis of the internal standard peak area. The percentage of test compound versus time was plotted and fitted by GraphPad Prism (GraphPad Software, Version 5 for Windows, CA, USA, www.graphpad.com) to estimate the compound's half-life ($t_{½}$) which was reported as mean value along with the standard deviation (*n = 3*).

4.7. Animals models

Male CD1 mice, weighing 22–24 g, were used (Charles River). All procedures were performed in accordance with the Ethical Guidelines of European Communities Council (Directive 2010/63/EU of September 22, 2010) and accepted by the Italian Ministry of Health. All efforts were made to minimize animal suffering and to use the minimal number of animals required to produce reliable results, according to the "3Rs concept". Animals were group-housed in ventilated cages and had free access to food and water. They were maintained under a 12-h light/dark cycle (lights on at 8:00 a.m.) at controlled temperature (21 °C ± 1 °C) and relative humidity (55% ± 10%).

4.8. Administration and experimental design

Compounds **1** and **2** were administered intravenously (IV) at 3 mg/kg. Vehicle was: PEG400/Tween 80/Saline solution at 10/10/80% in volume respectively. Three animals per each time point were treated. Blood samples and brains at 0, 5, 30, 60, 120 and 240 min after administration were collected.

Plasma was separated from blood by centrifugation for 15 min at 1500 rpm at 4 °C, collected in an eppendorf tube and frozen (−80 °C). Brain samples were homogenized in phosphate buffered saline and were then split in two aliquots kept at −80 °C until analysis. An aliquot was used for compound brain level evaluations, following the same procedure described below for plasma samples. The second aliquot was kept for protein content evaluation by bicinchoninic acid assay (BCA). Control animals treated with vehicle only were also included in the experimental protocol.

4.9. In vivo pharmacokinetic measurements

Plasma: Plasma samples were centrifuged at 21.100×*g* for 15 min at 4 °C. An aliquot of each plasma sample was extracted (1:3) with cold CH_3CN containing 200 nM of an appropriate internal standard. A calibration curve was prepared in blank mouse plasma over a 1 nM to 10 μM range. Three quality control samples were prepared by spiking the parent compound in blank mouse plasma to 20, 200 and 2000 nM as final concentrations. The calibrators and quality control samples were extracted (1:3) with the same extraction solution as the plasma samples. The plasma samples, calibrators and quality control samples were centrifuged at 3.270×*g* for 15 min at 4 °C.

Brain: Whole brains were homogenized in 4 vol (v/w) homogenizing solution (Phosphate Buffer Saline:Protease inhibitor (100:1)). An aliquot of each brain homogenate was extracted (1:3) with cold CH_3CN containing 200 nM of an appropriate internal standard. A calibration curve was prepared in naïve mouse brain homogenate over a 1 nM to 10 μM range. Three quality control samples were prepared by spiking the parent compound in naïve mouse brain homogenate to 20, 200 and 2000 nM as final concentrations. The calibrators and quality control samples were extracted (1:3) with the same extraction solution as the brain homogenates. The brain homogenates, calibrators and quality control samples were centrifuged at 3.270×*g* for 20 min at 4 °C.

Quantification: The supernatants of the extracted plasma samples, brain homogenates and respective calibrators and quality controls were further diluted (1:1) with H_2O, and analyzed by LC-MS/MS on a Waters ACQUITY UPLC-MS/MS system as defined above. All samples were quantified by MRM peak area response factor in order to determine the levels of the parent compound in both plasma and brain. The plasma concentrations versus time were plotted, and the profiles were fitted using PK Solutions Excel Application (Summit Research Service, USA) in order to determine the pharmacokinetic parameters.

Declaration of competing interest

The authors declare that they have no known competing financial interests or personal relationships that could have appeared to influence the work reported in this paper.

Data availability

Data will be made available on request.

Acknowledgments

This research was funded by the Italian Ministry of University and Research (MIUR), PRIN 2017(2017MT3993_007), Istituto Italiano di Tecnologia (IIT) and University of Nottingham.

Appendix A. Supplementary data

Supplementary data to this article can be found online at https://doi.org/10.1016/j.ejmech.2023.115803.

References

[1] P.T. Francis, The interplay of neurotransmitters in Alzheimer's disease, CNS Spectr. 10 (11 Suppl 18) (2005) 6–9, https://doi.org/10.1017/s1092852900014164.
[2] S. Teipel, D. Gustafson, R. Ossenkoppele, O. Hansson, C. Babiloni, M. Wagner, S. G. Riedel-Heller, I. Kilimann, Y. Tang, Alzheimer disease: standard of diagnosis, treatment, care, and prevention, J. Nucl. Med. 63 (7) (2022) 981–985, https://doi.org/10.2967/jnumed.121.262239.
[3] M.S. Uddin, A. Al Mamun, M.T. Kabir, G.M. Ashraf, M.N. Bin-Jumah, M.M. Abdel-Daim, Multi-target drug candidates for multifactorial alzheimer's disease: AChE and NMDAR as molecular targets, Mol. Neurobiol. 58 (1) (2021) 281–303, https://doi.org/10.1007/s12035-020-02116-9.
[4] J.P. Lopes, G. Tarozzo, A. Reggiani, D. Piomelli, A. Cavalli, Galantamine potentiates the neuroprotective effect of memantine against NMDA-induced excitotoxicity, Brain Behav 3 (2) (2013) 67–74, https://doi.org/10.1002/brb3.118.
[5] E. Simoni, S. Daniele, G. Bottegoni, D. Pizzirani, M.L. Trincavelli, L. Goldoni, G. Tarozzo, A. Reggiani, C. Martini, D. Piomelli, et al., Combining galantamine and memantine in multitargeted, new chemical entities potentially useful in Alzheimer's disease, J. Med. Chem. 55 (22) (2012) 9708–9721, https://doi.org/10.1021/jm3009458.
[6] A.M. Reggiani, E. Simoni, R. Caporaso, J. Meunier, E. Keller, T. Maurice, A. Minarini, M. Rosini, A. Cavalli, In vivo characterization of ARN14140, a memantine/galantamine-based multi-target compound for alzheimer's disease, Sci. Rep. 6 (2016), 33172, https://doi.org/10.1038/srep33172.
[7] M. Singhal, V. Merino, M. Rosini, A. Cavalli, Y.N. Kalia, Controlled iontophoretic delivery *in vitro* and *in vivo* of ARN14140 - a multitarget compound for alzheimer's disease, Mol. Pharm. 16 (8) (2019) 3460–3468, https://doi.org/10.1021/acs.molpharmaceut.9b00252.

[8] (a) B. Xiong, Y. Wang, Y. Chen, S. Xing, Q. Liao, Q. Li, W. Li, H. Sun, Strategies for structural modification of small molecules to improve blood-brain barrier penetration: a recent perspective, J. Med. Chem. 64 (18) (2021) 13152–13173, https://doi.org/10.1021/acs.jmedchem.1c00910;
(b) Z. Rankovic, CNS drug design: balancing physicochemical properties for optimal brain exposure, J. Med. Chem. 58 (6) (2015) 2584–2608, https://doi.org/10.1021/jm501535r.

[9] G.L. Ellman, K.D. Courtney, V. Andres, R.M. Feather-Stone, A new and rapid colorimetric determination of acetylcholinesterase activity, Biochem. Pharmacol. 7 (1961) 88–95, https://doi.org/10.1016/0006-2952(61)90145-9.

[10] M.L. Bolognesi, R. Banzi, M. Bartolini, A. Cavalli, A. Tarozzi, V. Andrisano, A. Minarini, M. Rosini, V. Tumiatti, C. Bergamini, et al., Novel class of quinone-bearing polyamines as multi-target-directed ligands to combat Alzheimer's disease, J. Med. Chem. 50 (20) (2007) 4882–4897, https://doi.org/10.1021/jm070559a.

[11] J. Cheung, M.J. Rudolph, F. Burshteyn, M.S. Cassidy, E.N. Gary, J. Love, M. C. Franklin, J.J. Height, Structures of human acetylcholinesterase in complex with pharmacologically important ligands, J. Med. Chem. 55 (22) (2012) 10282–10286, https://doi.org/10.1021/jm300871x.

[12] (a) N.H. Greig, T. Utsuki, Q. Yu, X. Zhu, H.W. Holloway, T. Perry, B. Lee, D. K. Ingram, D.K. Lahiri, A new therapeutic target in Alzheimer's disease treatment: attention to butyrylcholinesterase, Curr. Med. Res. Opin. 17 (3) (2001) 159–165, https://doi.org/10.1185/0300799039117057;
(b) T. Maurice, M. Strehaiano, N. Siméon, C. Bertrand, A. Chatonnet, Learning performances and vulnerability to amyloid toxicity in the butyrylcholinesterase knockout mouse, Behav. Brain Res. 296 (2016) 351–360, https://doi.org/10.1016/j.bbr.2015.08.026;
(c) M. Hoffmann, C. Stiller, E. Endres, M. Scheiner, S. Gunesch, C. Sotriffer, T. Maurice, M. Decker, Highly selective butyrylcholinesterase inhibitors with tunable duration of action by chemical modification of transferable carbamate units exhibit pronounced neuroprotective effect in an alzheimer's disease mouse model, J. Med. Chem. 62 (20) (2019) 9116–9140, https://doi.org/10.1021/acs.jmedchem.9b01012.

[13] (a) S. Darvesh, D. Hopkins, C. Geula, Neurobiology of butyrylcholinesterase, Nat. Rev. Neurosci. 4 (2) (2003) 131–138, https://doi.org/10.1038/nrn1035;
(b) A. Ciro, J. Park, G. Burkhard, N. Yan, C. Geula, Biochemical differentiation of cholinesterases from normal and Alzheimer's disease cortex, Curr. Alzheimer Res. 9 (1) (2012) 138–143, https://doi.org/10.2174/156720512799015127.

[14] N. Greig, T. Utsuki, D. Ingram, Y. Wang, G. Pepeu, C. Scali, Q. Yu, J. Mamczarz, H. Holloway, T. Giordano, et al., Selective butyrylcholinesterase inhibition elevates brain acetylcholine, augments learning and lowers Alzheimer beta-amyloid peptide in rodent, Proc. Natl. Acad. Sci. U.S.A. 102 (47) (2005) 17213–17218, https://doi.org/10.1073/pnas.0508575102. Article.

[15] F. Nachon, E. Carletti, C. Ronco, M. Trovaslet, Y. Nicolet, L. Jean, P. Renard, Crystal structures of human cholinesterases in complex with huprine W and tacrine: elements of specificity for anti-Alzheimer's drugs targeting acetyl- and butyryl-cholinesterase, Biochem. J. 453 (2013) 393–399, https://doi.org/10.1042/BJ20130013. Article.

[16] (a) G.E. Hardingham, Y. Fukunaga, H. Bading, Extrasynaptic NMDARs oppose synaptic NMDARs by triggering CREB shut-off and cell death pathways, Nat. Neurosci. 5 (5) (2002) 405–414, 10.1038/nn835;
(b) Y. Liu, T.P. Wong, M. Aarts, A. Rooyakkers, L. Liu, T.W. Lai, D.C. Wu, J. Lu, M. Tymianski, A.M. Craig, et al., NMDA receptor subunits have differential roles in mediating excitotoxic neuronal death both in vitro and in vivo, J. Neurosci. 27 (11) (2007) 2846–2857, https://doi.org/10.1523/JNEUROSCI.0116-07.2007.

[17] P. Xia, H.S. Chen, D. Zhang, S.A. Lipton, Memantine preferentially blocks extrasynaptic over synaptic NMDA receptor currents in hippocampal autapses, J. Neurosci. 30 (33) (2010) 11246–11250, https://doi.org/10.1523/JNEUROSCI.2488-10.2010.

[18] (a) M. Rosini, E. Simoni, R. Caporaso, F. Basagni, M. Catanzaro, I.F. Abu, F. Fagiani, F. Fusco, S. Masuzzo, D. Albani, et al., Merging memantine and ferulic acid to probe connections between NMDA receptors, oxidative stress and amyloid-β peptide in Alzheimer's disease, Eur. J. Med. Chem. 180 (2019) 111–120, https://doi.org/10.1016/j.ejmech.2019.07.011;
(b) M. Kaniakova, E. Nepovimova, L. Kleteckova, K. Skrenkova, K. Holubova, Z. Chrienova, V. Hepnarova, T. Kucera, T. Kobrlova, K. Vales, et al., Combination of memantine and 6-chlorotacrine as novel multi-target compound against alzheimer's disease, Curr. Alzheimer Res. 16 (9) (2019) 821–833, https://doi.org/10.2174/1567205016666190228122218;
(c) Z. Gazova, O. Soukup, V. Sepsova, K. Siposova, L. Drtinova, P. Jost, K. Spilovska, J. Korabecny, E. Nepovimova, D. Fedunova, et al., Multi-target-directed therapeutic potential of 7-methoxytacrine-adamantylamine heterodimers in the Alzheimer's disease treatment, Biochim. Biophys. Acta, Mol. Basis Dis. 1863 (2) (2017) 607–619, https://doi.org/10.1016/j.bbadis.2016.11.020.

[19] D. Stroebel, D.L. Buhl, J.D. Knafels, P.K. Chanda, M. Green, S. Sciabola, L. Mony, P. Paoletti, J. Pandit, A novel binding mode reveals two distinct classes of NMDA receptor GluN2B-selective antagonists, Mol. Pharmacol. 89 (5) (2016) 541–551, https://doi.org/10.1124/mol.115.103036.

[20] (a) P. Webborn, The role of pharmacokinetic studies in drug discovery: where are we now, how did we get here and where are we going? Future Med. Chem. 6 (11) (2014) 1233–1235, https://doi.org/10.4155/FMC.14.76. Editorial Material;
(b) T.N. Thompson, Early ADME in support of drug discovery: the role of metabolic stability studies, Curr. Drug Metabol. 1 (3) (2000) 215–241, https://doi.org/10.2174/1389200003339018.

[21] L. Di, E.H. Kerns, X.J. Ma, Y. Huang, G.T. Carter, Applications of high throughput microsomal stability assay in drug discovery, Comb. Chem. High Throughput Screen. 11 (6) (2008) 469–476, https://doi.org/10.2174/138620708784911429.

[22] R. Scott Obach, Functional group biotransformations, in: Handbook of Metabolic Pathways of Xenobiotics, 2014, pp. 1–41.

[23] T.T. Wager, X. Hou, P.R. Verhoest, A. Villalobos, Central nervous system multiparameter optimization desirability: application in drug discovery, ACS Chem. Neurosci. 7 (6) (2016) 767–775, https://doi.org/10.1021/acschemneuro.6b00029.

[24] (a) T.A. Halgren, R.B. Murphy, R.A. Friesner, H.S. Beard, L.L. Frye, W.T. Pollard, J.L. Banks, Glide: a new approach for rapid, accurate docking and scoring. 2. Enrichment factors in database screening, J. Med. Chem. 47 (7) (2004) 1750–1759, https://doi.org/10.1021/jm030644s;
(b) R.A. Friesner, J.L. Banks, R.B. Murphy, T.A. Halgren, J.J. Klicic, D.T. Mainz, M. P. Repasky, E.H. Knoll, M. Shelley, J.K. Perry, et al., Glide: a new approach for rapid, accurate docking and scoring. 1. Method and assessment of docking accuracy, J. Med. Chem. 47 (7) (2004) 1739–1749, https://doi.org/10.1021/jm0306430.

[25] R.A. Friesner, R.B. Murphy, M.P. Repasky, L.L. Frye, J.R. Greenwood, T.A. Halgren, P.C. Sanschagrin, D.T. Mainz, Extra precision glide: docking and scoring incorporating a model of hydrophobic enclosure for protein-ligand complexes, J. Med. Chem. 49 (21) (2006) 6177–6196, https://doi.org/10.1021/jm051256o.

[26] W. Sherman, T. Day, M.P. Jacobson, R.A. Friesner, R. Farid, Novel procedure for modeling ligand/receptor induced fit effects, J. Med. Chem. 49 (2) (2006) 534–553, https://doi.org/10.1021/jm050540c.

[27] M.P. Jacobson, D.L. Pincus, C.S. Rapp, T.J. Day, B. Honig, D.E. Shaw, R.A. Friesner, A hierarchical approach to all-atom protein loop prediction, Proteins 55 (2) (2004) 351–367, https://doi.org/10.1002/prot.10613.

[28] C. Lu, C. Wu, D. Ghoreishi, W. Chen, L. Wang, W. Damm, G.A. Ross, M.K. Dahlgren, E. Russell, C.D. Von Bargen, et al., OPLS4: improving force field accuracy on challenging regimes of chemical space, J. Chem. Theor. Comput. 17 (7) (2021) 4291–4300, https://doi.org/10.1021/acs.jctc.1c00302.